DEPARTMENT OF MECHANICAL & AEROSPACE ENGINEERING

University of Strathclyde Engineering

An Investigation into the orbital lifetime and passive disposal of global navigation satellites in medium Earth orbit

Jacob Currie

Supervisor: Dr Jinglang Feng

A thesis submitted in partial fulfilment of the requirements of the Aero-Mechanical Engineering BEng degree at the University of Strathclyde

2021

Word count: 8,680 words

Abstract

The increasing number of space missions and space vehicle launches, as a result of humanities growing dependence on technological infrastructure in space, has resulted in a substantial amount of space debris, that poses a threat of collision to operational satellites. Various collisions and problems caused by space debris have been observed previously, suggesting that a solution for removing debris and mitigating further deposits is needed. This thesis provides a proof of concept, for a possible solution that inhibits further contributions of space debris to orbit, via an economically and technically feasible, passive deorbiting strategy.

This strategy centralises the concept of predetermined disposal orbits, which are inherently unstable by choice and will result in re-entry and disposal of debris within a short time span. This is possible due to various perturbing influences that cause a satellite's orbit to drift and evolve over time, causing the satellite to re-enter Earth's atmosphere and burn up. This thesis aims to investigate the orbital dynamics of the Medium Earth Orbit region, specifically the location of the current global navigation satellite systems, in order to locate possible disposal orbit solutions for these constellations, and evaluate the feasibility of a passive disposal strategy overall for the observed regions.

This paper constructed a hypothetical map of the navigational satellite region, via the propagation of a large number of orbits with use of a numerical integration scheme, implemented in MATLAB, for a variety of initial conditions, taking into account the most significant sources of orbital perturbation, highlighted in the relevant literature.

The results showed that a considerable number of feasible disposal orbits exist in the region, presenting in discrete clusters at specific inclinations, with areas of distinct abundance and sparsity, with the perturbing influence of solar radiation pressure having an enhancing effect on the disposal feasibility and deorbit time. and concluded that a feasible passive end-of-life disposal solution exists for the studied region.

Student No. 201718558

Contents

Table of Figures

Table of Tables

Table of Abbreviations

Abbreviation	Meaning
MEO	Medium Earth Orbit
LEO	Low Earth Orbit
GEO	Geostationary Orbit
SRP	Solar Radiation Pressure
GNSS	Global Navigation Satellite System (Generic)
GPS	Global Positioning System
GLONASS	Global Navigation Satellite System (Russian Satellite)

Nomenclature

Quantities in bold are representative of vectors

Symbol	Description	Units
μ	Earth's gravitational parameter (GM)	m^3/s^2
$\mathbf{a}_{Earth}$	Earth's gravitational acceleration	km/s^2
$\mathbf{a}_{Moon}$	Lunar perturbing acceleration vector	km/s^2
A_{ratio}	Area-to-mass ratio	
$\mathbf{a}_{sat}$	Net acceleration of satellite	km/s^2
$\mathbf{a}_{SRP}$	SRP perturbing acceleration vector	km/s^2
$\mathbf{a}_{Sun}$	Solar perturbing acceleration vector	km/s^2
c	Speed of light	m/s
C_r	Coefficient of reflectivity	
F_{Earth}	Earth's gravitational force	N
F_{J2}	J2 perturbing force	N
F_{Moon}	Moon's gravitational force	N
F_{sat}	Net force acting on satellite	N
F_{SRP}	Solar radiation pressure force	N
F_{Sun}	Sun's gravitational force	N
G	Gravitational constant	$m^3/kg\ s^2$
HP	Lunar horizontal parallax	°
J_2	J_2 zonal harmonic coefficient	
L_s	Mean solar longitude	°
m_{Earth}	Mass of Earth	kg
m_{Moon}	Mass of the Moon	kg
M_s	Mean solar anomaly	°
m_{Sun}	Mass of the Sun	kg
n	Number of Julian days after J2000	
$\mathbf{P}_{J2}$	Perturbing acceleration from J_2	km/s^2
R	Earth's equatorial radius	km
r	Satellite displacement magnitude	km
r_m	Lunar displacement magnitude	km
$\mathbf{r}_m$	Lunar position vector	km
r_s	Solar displacement magnitude	km
S	Solar constant	W/m^2
T_0	Number of Julian centuries after J2000	
$\mathbf{u}_s$	Solar position vector	km
$\mathbf{u}_{SRP}$	Sun-to-satellite direction vector	
v	Shadow function	
δ_m	Lunar ecliptic latitude	°
ε_m	Lunar obliquity to the ecliptic plane	°
ε_s	Solar obliquity	°
λ_a	Apparent solar longitude	°
λ_m	Lunar ecliptic longitude	°

1.0 Introduction

1.1 Background

Space debris has been a concern since humanity embarked on its first space-reaching venture, with numerous manned and unmanned missions leaving residual debris in orbit, contributing to a large chaotic cloud of non-manoeuvrable objects in a wide range of orbital positions. As the technological abilities of mankind inevitably advance at an ever-increasing rate, is important that space debris does not become a hindrance to technological progress as humanity pushes to become a space-conquering species. Therefore, it is important to develop economical and effective mitigation strategies for debris. This can be achieved in a variety of ways, some more cost-effective than others, it is unfeasible to imagine an active “debris clean-up” approach, whereby debris is captured and removed from orbit via an external method or machine. However, passive strategies have been theorised and developed to provide an effective solution to de-orbiting space debris, by predicting the orbital path of the object to determine if and when it will leave Earth’s orbit or be destroyed by natural re-entry. In the case of removing a piece of debris that still retains manoeuvrability, i.e., a satellite that has reached the end of its service life, it is possible to move the satellite onto a predetermined “disposal” orbit, where it will perform re-entry much sooner than if it were left undisturbed. Figure 1 below shows the exponential increase in total space debris in recent years.

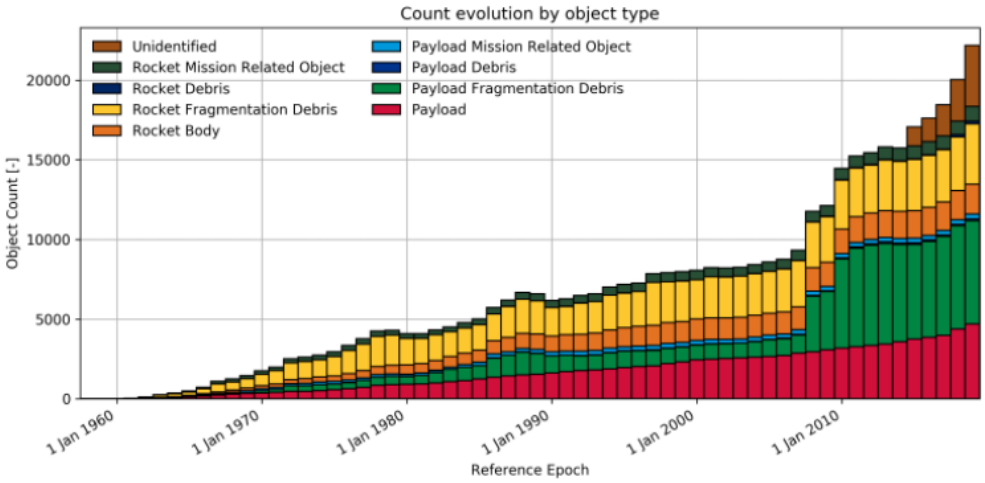

Figure 1 - Distribution of Space Debris across Time[1]

1.2 Problem Description

In order to investigate and analyse the orbital lifetime and stability of a satellite’s orbit, a suitable dynamical model must first be developed in order to propagate the orbits across a chosen time span, before being implemented into an appropriate software package to allow for efficient computation of an orbit for any initial satellite position. This will allow for the generation of results across a wide range of initial conditions, which can in turn be used to create visual representations of the data for analysis.

1.3 Thesis Objectives

This thesis aims to achieve the following objectives:

- Research and identify the important perturbing influences throughout Earth's orbital space by investigating the relevant literature.
- Investigate and study the related academic literature to learn about the distribution of space debris.
- Develop an appropriate mathematical model that can be used to propagate a satellite's orbit around Earth for a given time span.
- Define the geographic orbital range of space that will be investigated using the mode.
- Implement the model into the MATLAB programming environment to allow for computation of results.
- Use an appropriately comparable trusted model of similar design, to validate the model and verify the accuracy of the results.
- Create visual representations of the results in the form of contour plots for analysis.
- Critically analyse the generated results to identify any disposal orbit regions in the investigated region, and evaluate the feasibility and cost of their use.

1.4 Project Scope

This project focuses specifically on the medium Earth orbit ("MEO") region of Earth's orbital space, with an emphasis on the orbital regions occupied by the world's current global navigation satellite system ("GNSS") constellations. These constellations are strategically positioned for optimum coverage of their respective countries or regions for providing global positioning and navigation information services to users on the surface. GNSS satellite constellations are of great importance for the function of many common civilian and military services and devices, for example: all modern smartphones use satellite positioning for a variety of reasons, as well as all modern aircraft, which feature satellite navigation systems within their autopilot systems in civilian use cases, and for weapons targeting systems in military use cases. The GNSS orbital region is a prime candidate for space debris, as technological advances begin to force upgrades and expansions on these GNSS constellations. Therefore, it is important to have a sustainable and economical strategy for dealing with these constellations once they reach the end of their service life, and eliminate contributions to space debris.

2.0 Literature Review

As an increasing number of satellites are launched into orbit each year, the current operating region of space is becoming increasingly populated with both operational satellites, and many forms of debris such as rocket bodies, broken satellites, lost equipment from manned missions, and ejected shrapnel debris from orbital collisions. This cloud of debris poses a significant threat of collision and damage to current satellites in service and future launches, as well as prohibiting the use of certain orbits, due to space debris occupying such a large area of the orbital plane. Inanimate, uncontrollable debris such as spent rocket boosters, are very difficult and costly to remove as they require external intervention in order to change their orbit, while operational satellites that possess manoeuvrability can be disposed of relatively safely and with much less expense and resources, this is possible through a passive dynamical approach where the satellite's orbit is manipulated so that it performs a long-term manoeuvre resulting in re-entry or the satellite reaching a graveyard orbit. It has become clear through the increase in space debris and previous research into this problem that a plan for space debris mitigation is necessary in future planned missions.

2.1 Geocentric Space Regions

As humanity has researched and explored further from Earth's surface into outer space, various regions have been defined to aid in the classification of satellites and their orbits: Low Earth Orbit ("LEO"), Medium Earth Orbit ("MEO"), Geosynchronous Orbit ("GEO"). Currently, the LEO and GEO regions have been placed under a protected status[2], meaning that any satellites placed in orbit inside these regions should have effective space debris mitigation strategies in place. However, the MEO region is not under any protective cover[2]. The LEO region covers altitudes up to 2,000km, while the GEO region is defined at an altitude of 35,786km ± 200km, the MEO region occupies the altitudes between the two[2].

2.2 Current GNSS Constellations

There are currently four major GNSS constellations operational in the MEO region, the USA's global positioning system ("GPS"), Russia's global navigation satellite system ("GLONASS"), the European Space Agency's "Galileo" GNSS constellation, and China's "Beidou" constellation. All of these constellations operate in similar area and are all in close proximity to each other in terms of their orbital parameters. The layout of Galileo is shown below in figure 2.

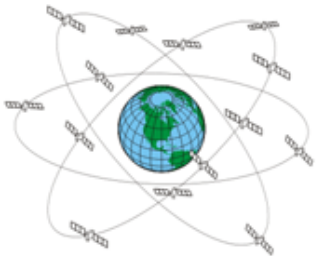

Figure 2 - Diagram of Galileo GNSS Constellation[3]

2.2.1 Global Positioning System (GPS)

Development of the GPS system, originally known as “NavStar”, started in 1973, and uses a system of 6 circular orbital planes, each home to 4 satellites, for a total of 24 in-service satellites, which give the GPS constellation full functionality. Each orbital plane is inclined at an angle of 55° relative to Earth’s equator, at an altitude of 20,200km[4] and this is the only constellation in which the satellites are not evenly spaced around their orbital planes. The GPS constellation is the oldest of the world’s GNSS systems, and as a result of its long lifespan and numerous upgrades and changes, has contributed 41 retired or non-functional satellites to space debris.

2.2.2 Global Navigation Satellite System (GLONASS)

The GLONASS constellation, originally developed by the Soviet Union in 1976, as an answer to the USA’s GPS system, is a system of 3 circular orbital planes, with a total of 24 satellites giving full operation, split evenly with 8 satellites in each plane, evenly spaced at 45° apart within their respective planes. The GLONASS satellites orbit at an altitude of 19,100km, with their orbital planes inclined at an angle of 64.8°[4]. The GLONASS system was subject to many revisions and upgrades across 3 generations, which resulted in 105 retired or non-functional satellites contributing to space debris in the MEO region

2.2.3 Galileo GNSS Constellation

The Galileo constellation, built and maintained by the European Space Agency for the European Union, with completion in 2016, consists of 24 satellites split equally into groups of 8 in 3 orbital planes at an inclination of 56°. The system is still in development and has satellite launches planned for 2021[5] that will bring improvements to the system. The operating altitude of the constellation is 23,222km[4]. With its more recent construction and development, the Galileo GNSS project has resulted in 4 satellites that have been categorised as debris.

2.2.4 Beidou GNSS Constellation

The Beidou constellation, designed and built by China to provide more accurate navigational coverage to its nation and the surrounding region, consists of 27 satellites split across 3 orbital planes with an inclination of 55°, and an altitude of 21,500km[4]. Beidou-3 was recently completed in June of 2020, replacing an older constellation, Beidou-1, which was decommissioned in 2012, followed by Beidou-2, which is still in partial operation alongside its updated third generation sibling. Over the course of Beidou’s construction and upgrade projects, 17 non-operational satellites have been launched and categorised as debris. The Beidou system also additionally occupies 1 geostationary orbital plane containing 5 satellites.

2.3 Space Debris Distribution in MEO

The complex distribution of space debris throughout the MEO region is a result of many influencing factors from chosen satellite launch locations and orbits creating clusters of man-made vehicles and objects with similar orbital parameters, and external forces from the Sun, Moon, and other celestial bodies modifying the distribution of debris as it orbits Earth.

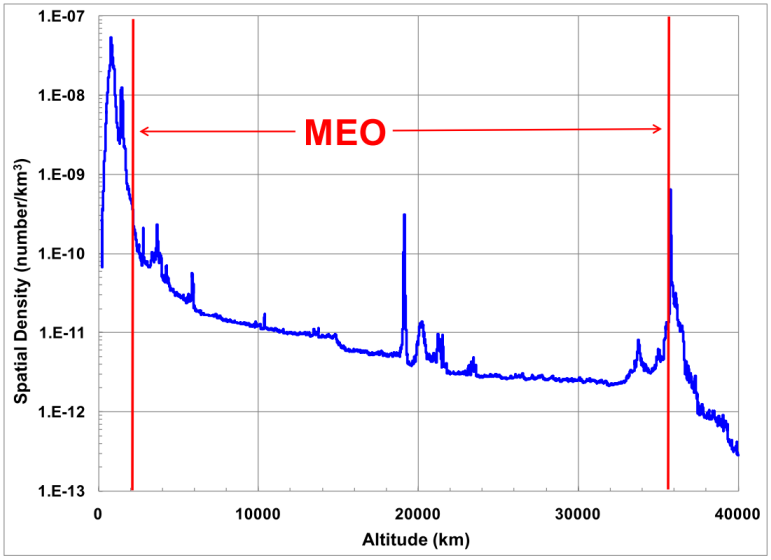

Figure 3 - Spatial Density of Debris with respect to Altitude[6]

The above figure 3 shows the spatial density of debris distribution across the MEO region, it is clear that the debris is unevenly distributed, with a large quantity present close to the lower MEO altitude limit, and a large cluster of debris around the altitude of 19,000km (this is likely representing the large number of non-functional GLONASS vehicles). The continuous distribution across the entire MEO region shows that there is no distinct area of immense concentration that could be targeted in an efficient manner, the debris problem is present throughout the region. Due to the significantly larger volume of the MEO region, relative to the other regions, the average threat of collision is significantly lower also[6]. The concern is that without mitigation strategies, and the growing trend of increasing the size and complexity of GNSS constellations to meet technological demand, the debris density could rise to much more dangerous levels, increasing the difficulty of technological advancement in the GNSS sector and the risk to the constellations in the long term.

2.4 Current Disposal Strategies

With the increasingly imposing threat from space debris receiving more attention in recent years, a number of strategies and concepts have been theorised to help deal with the problem, ranging from active debris clean-up programs to legislation that will assist in the mitigation of debris in the future. The most viable solution centralises the idea of passive debris removal, utilising the dynamical effects of the MEO region to deorbit satellites without external intervention.

2.4.1 Active Disposal Concepts

While concepts and vehicles designed to actively “reach out” and remove space debris from orbit, have been developed, and a mission to launch a single-use large debris deorbiting vehicle “ClearSpace-1” has been planned for 2025[7]. No successful active debris disposal effort has been carried out, this is due to the extremely large cost and effort required for such a project, it has however been proven to be possible and technologically feasible[8], for debris in the LEO region, and with a multi-use vehicle, raising the efficiency of the mission significantly.

2.4.2 Passive Disposal Approach

For debris in the MEO region, the most feasible strategy for the mitigation of space debris is with a passive approach, as the debris in the MEO region is much more sparsely distributed, an active solution is far less feasible and more expensive. A passive solution involves manoeuvring a satellite from its original position, onto a predetermined “disposal” orbit, which is unstable by design, and will result in the satellite deorbiting either via re-entry and eventual burnup in Earth’s atmosphere, or by sending the satellite on a path out to a graveyard orbit, the former being preferred as it results in the complete removal of the satellite, rather than just pushing the debris farther away. The instability of disposal orbits is due to a number of perturbations that induce an evolution of the orbit over time, this can result in the orbit becoming highly elliptical and cause it to precess around Earth, resulting in its eventual re-entry.

The instability of a disposal orbit, results in the growth of the orbits eccentricity[9], causing its elliptical path to stray increasingly farther from circular, causing the satellites altitude to oscillate between continuously widening maximum and minimum values. Once the minimum altitude value reaches a small enough value, the satellite will perform re-entry due to Earth’s atmosphere.

Investigations into finding feasible disposal orbits have carried out, a study into the dynamical characteristics of the MEO region from 2019[10] found that “the most interesting and complex dynamical behaviour appears for moderate-to-high inclinations ($\sim 40° - 70°$), where the GNSS groups are actually placed.”. And found there were some disposal orbits available in close proximity to the orbits of current GNSS constellations, with reasonable energy requirements for a transfer to these disposal orbits.

It is clear that there is feasibility for a passive debris mitigation strategy, whereby the end-of-life disposal strategy is predetermined during the development of the satellite, with enough energy stored to perform the manoeuvre to a suitable disposal orbit. It has been shown that disposal strategy compliance legislation could reduce collision rates across all regions by an average of 30%[11].

2.5 Sources of Orbital Perturbation

The most significant sources of perturbing influence, that cause an object's orbit to drift from its desired unchanging location, when in the MEO region, are the oblate shape of the Earth, gravitational forces from the Sun and Moon, and the pressure of direct solar radiation[12]. This is visualised in figure 4 below[12], showing the perturbing acceleration magnitude as a function of altitude.

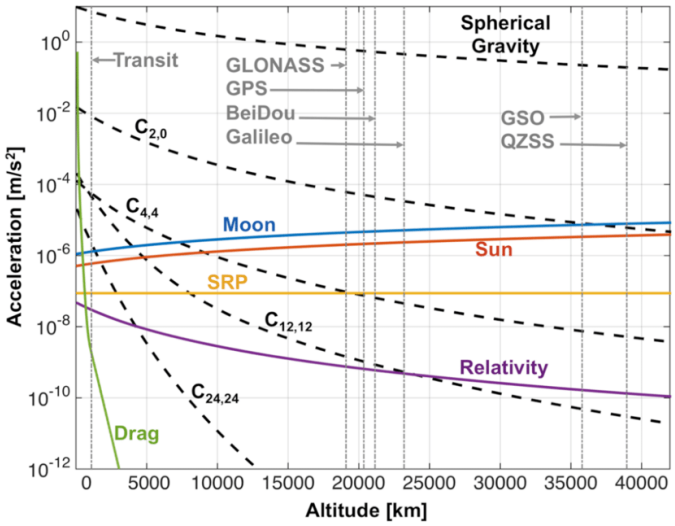

Figure 4 - Perturbation Acceleration as a Function of Orbital Altitude

While the magnitudes of these forces are relatively unchanging, their directions are in constant change and their effect on an orbiting body cannot be described simply, therefore, in order to investigate the evolution of the body's position, it must be propagated with a mathematical model.

2.5.1 Earth's Oblateness

Earth's "squished" oblate shape causes orbits to precess around Earth's polar axis[13], this does not inherently cause instability, but is an important factor as it does result in the satellite's Earth relative position changing over time. This effect has been documented previously, and various models have been created to describe it mathematically, the most common of which is the "J2" perturbator, which approximates the Earth's gravity based on as an oblate spheroid. Some more complex models have been developed that account for region specific variations in Earth's geopotential, such as "EGM96"[14] shown in figure 5, which accurately approximates subsurface variations in gravitational potential. However, this type of model is very complex and often not relevant for use in high altitude orbital applications, the oblate spheroid model can provide an appropriate approximation.

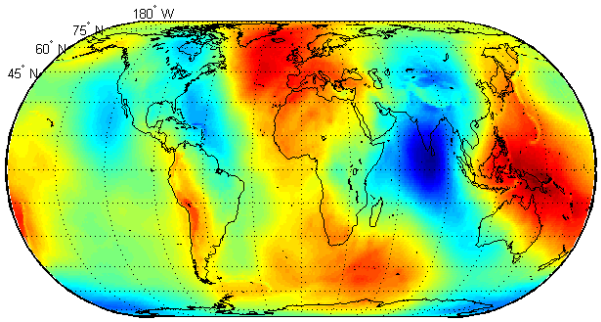

Figure 5 - EGM96 Geopotential Model[14]

2.5.2 Lunisolar Resonance

Gravitational perturbing forces from the Sun and Moon result in complex time dependant effects that cannot be described absolutely[15], The resulting effects are unstable and unpredictable, and it has been found that “these resonances lead to very different behaviour of the orbital evolution over time, even though initial parameters might have been very similar.”[16]. As a consequence, these effects must be modelled simultaneously when propagating an orbit. The lunisolar perturbing force has been shown to induce variation in the eccentricity or “circularity” of a satellite’s orbit, as well as causing overall drift in its position[10]. The effects of lunisolar resonances has a strong dependence on the initial orientation of the satellite for a given point in time[17]. Previous studies have found many feasible disposal orbits with low eccentricity, close to the inclination of GNSS constellations[17]. It has also been shown that the perturbing impact of lunisolar resonance is highly dependent on the satellites inclination[16].

2.5.3 Solar Radiation Pressure

Direct solar radiation pressure (“SRP”), while the least significant perturbing effect, has the unique property of only being active while the orbiting body has direct line-of-sight to the Sun. The perturbing effect from SRP has been shown to not significantly alter the orbital state of a satellite positioned at similar inclinations to the GNSS constellations, rather it has an amplifying effect on the growth of instability, causing a satellite to deorbit faster, with a relatively unchanged path[17].

2.6 Characteristics of the MEO region

A perturbing influence with little to no impact in the MEO region is that of atmospheric drag, with 99.9999% of Earth's atmosphere lying below an altitude of 100km[18]. As the atmosphere is only considered to exist up to 1000km[18], satellites in MEO are not subject to aerodynamic drag, although objects in LEO do have to contend with a constant drag force that decays exponentially with altitude. For objects in LEO with an altitude of 1000km, the drag force is almost non-existent, due to the very low air density (3.5e-15). However, at altitudes lower than this, like that of current satellites such as the International Space Station (400km), and the Hubble Space Telescope (560km), atmospheric drag is of such importance that frequent corrections or "boosts" of the orbits are required such that they do not perform re-entry prematurely.

The resonances that result in the instability of an orbit have been shown to be densely packed around the GNSS inclination values[19], inferring that there is a lot of potential for chaotic perturbation and seemingly random resulting orbital evolution. The figure 6 below shows the closely packed nature of the centres of the lunisolar resonance harmonics for a semimajor axis of 29,600km[19]. It should be noted that the structures share significant similarity across variation of the semimajor axis. This shows that the influence of lunisolar resonance is most prominent at inclinations between 45 and 75 degrees.

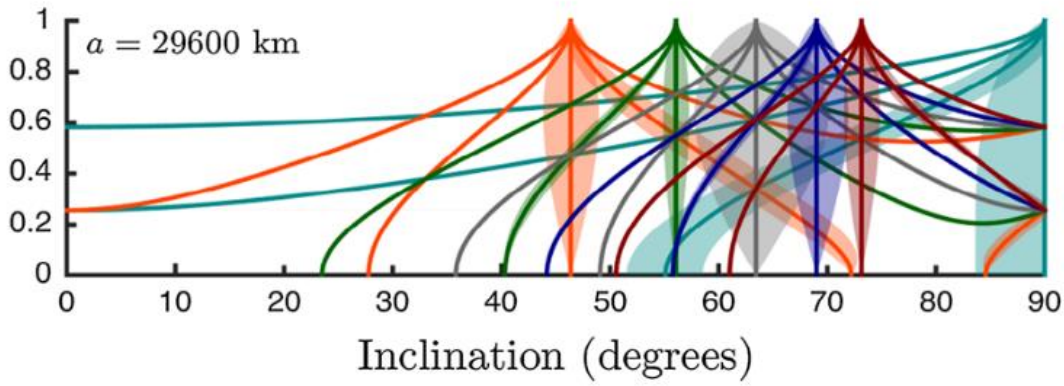

Figure 6 - Lunisolar Resonance Structure/Centres as a function of eccentricity and inclination[19]

2.7 Orbit Propagation Strategies

Many software tools have previously been developed to serve the purpose of orbit propagation with consideration for complex perturbations, while the most advanced propagation systems created to serve the needs of governmental powers for use in military applications are not available to the public, readily available solutions have been developed for both individual and commercial use. The most notable "off-the-shelf" software applications available are discussed below.

2.7.1 NASA's GMAT

The General Mission Analysis Tool ("GMAT"), developed by NASA and released for free public use, is an open-source space mission development software suite that features precise orbit propagation capabilities for geocentric satellites as well as deep space interstellar missions. It is a fully featured software application designed for a wide set of use cases. GMAT propagates orbits using numerical integration, with a choice of methods available catering to different levels of precision, such as the "Runge-Kutta56" method, and the Adams-Bashforth-Moulton method[20], also used by MATLAB's "ODE113" integrator. GMAT also features easy implementation of orbital perturbations, with baked in support for complex geopotential models, as well as user-defined SRP models. GMAT is currently under continuous development with a number of bugs and errors still present in certain areas[20].

2.7.2 A.I. Solutions' FreeFlyer

"FreeFlyer" is a proprietary mission design tool very similar to GMAT, developed by A.I Solutions, it requires a commercial license to use, which accompanies extensive documentation and support. It supports advanced perturbation modelling with the inclusion of complex geopotential models as well as atmospheric density models for use with calculating aerodynamic drag, the International Reference Ionosphere model, and the International Geomagnetic Reference Field, to aid in the development of electronic systems in orbit. FreeFlyer uses its own scripting language for development, known as FreeForm, similar in syntax to MATLAB's own scripting language. While fully capable of precise orbit propagation, FreeFlyer is a spacecraft-oriented design tool, focusing on the development and optimisation of on-spacecraft systems, such as solar arrays, or mission specific sensory and antenna systems, as well as spacecraft manoeuvre dynamics[21]. The orbit propagation system present in FreeFlyer uses the same numerical integration methods as GMAT, incorporating the "Runge-Kutta89" method among others[22].

2.7.3 AGI's Systems Tool Kit

The Systems Tool Kit (STK) developed by AGI, a subsidiary of Ansys, Inc. since 2020. Is most similar to FreeFlyer in its publication, being a proprietary commercial application that requires a license for use. It also shares similarities to FreeFlyer in its design, featuring the same capabilities in terms of orbit propagation, and being a spacecraft-oriented design system, for use in developing vehicle subsystems, rather than an orbit-focused dynamical analysis tool. The capabilities of STK extend to the development of land and sea-based systems also, being described as a tool that "enables engineers and scientists to perform complex analyses of ground, sea, air, and space platforms" by its creators[23].

3.0 Method

3.1 Mathematical Model

To develop the dynamical model describing the motion of a satellite in orbit around Earth, a free body diagram was constructed, considering the gravitational force from the Earth, as well as how its oblate shape creates discrepancies from the point mass gravity approximation, and also the gravitational forces from the Sun and Moon, and the direct solar radiation pressure ("SRP") from the Sun, while neglecting air resistance, this is shown in figure 7 below. The resulting equation derived from Newton's 2nd law describing the forces acting on the satellite, is shown below.

$$\sum F_{sat} = F_{Earth} + F_{J2} + F_{Sun} + F_{Moon} + F_{SRP} \quad (1)$$

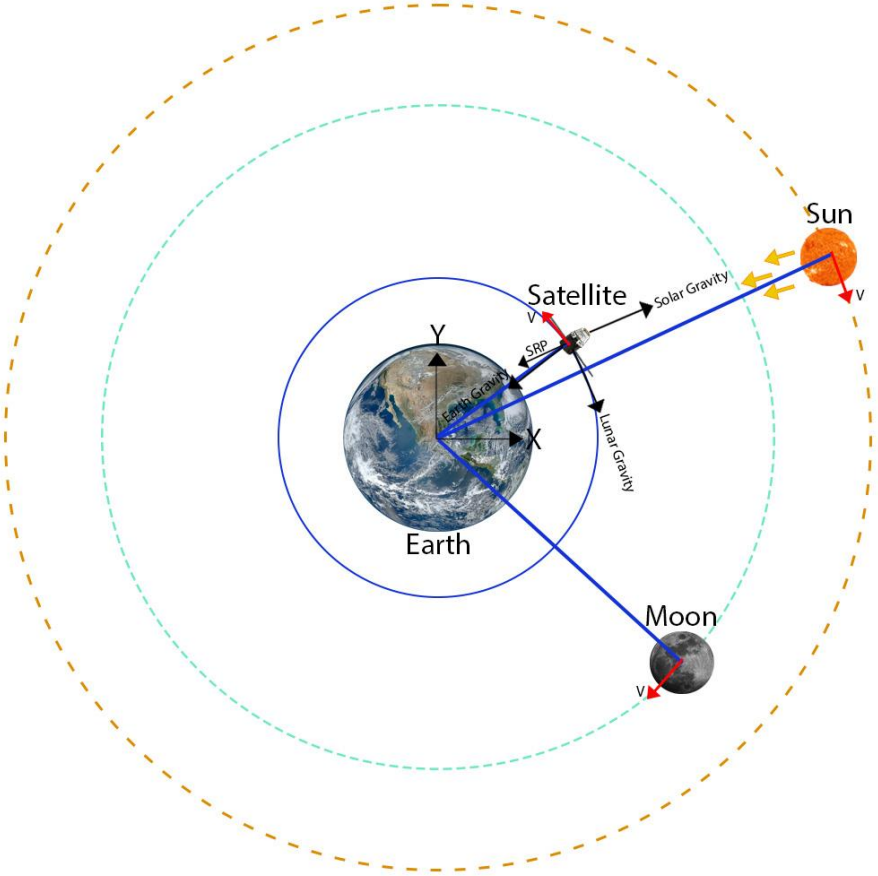

Figure 7 - Free body diagram of satellite and external system of bodies

3.2 Coordinate Systems

Coordinate system and reference frame choice was of high importance when constructing the mathematical model, as consistency throughout the various subsections of the model is key to ensuring accurate results, various transformations between different coordinate systems are used during calculation of lunar and solar positional data, this is explained in the individual sections describing the perturbing forces in the model.

3.2.1 Model Coordinate System

The mathematical model in this thesis uses a cartesian coordinate system in a geocentric inertial reference frame, with the Z-axis defined as the Earth's polar axis (normal to the equatorial plane), the X-axis at 0° longitude (Greenwich), and the Y-axis at 90°, at the initial starting epoch of the model simulation.

3.2.2 Orbital Elements Coordinate System

To fully define and easily describe any satellite's orbital path, the system of 6 orbital elements, devised by Kepler, are used. These parameters allow for a simple definition of an orbit, that can be easily interpreted for comparison and correlation with results. These parameters can also be used to generate "state vectors" in the traditional cartesian coordinate system, which are two vector quantities describing the satellite's position and velocity, allowing for easy conversion between coordinate systems. A set of state vectors also fully describe a satellites orbital state. The system of orbital elements is defined below.

- Semimajor axis, the distance between the furthest point of the orbit and the centre of the orbital ellipse.
- Eccentricity, a measure of how circular or elliptical an orbit is.
- Inclination, the angle at which the orbital plane is inclined from the reference plane.
- Longitude of the ascending node, the angle measured around an axis normal to the reference plane, to the point where the orbital path crosses through the reference plane. This point is known as the ascending node.
- Argument of periapsis, the angle measured in the orbital plane, between the reference plane and the point of periapsis (the point at which the satellite is closest).
- True anomaly, the angle measured between the periapsis line and the point at which the satellite is currently positions along its orbit.

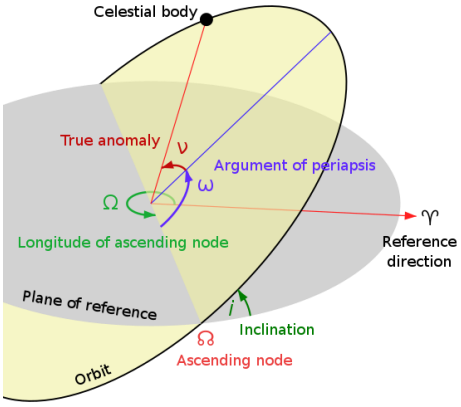

Figure 8 - Coordinate system diagram of Orbital Elements[24]

3.3 Oblate Spheroid Earth Model

In order to account for Earth's oblateness, a special perturbation is added as a modifier to Newton's point mass approximation of Earth's gravity, this term describes the perturbing force on the satellite due to this geopotential variation, in this model the "J_2" perturbator is used, which approximates the perturbing effect of a rotationally symmetric oblate mass, the resulting equation that describes this effect is given by an infinite series, however the most significant term by 3 orders of magnitude is the term known as J_2, therefore that term alone is used for the oblateness model in this case. The equation for the perturbing acceleration acting on the satellite (2) is given below[18].

$$\boldsymbol{p}_{J2} = \frac{3}{2}\frac{J_2 \mu R^2}{r^4}\left[\frac{x}{r}\left(5\frac{z^2}{r^2}\right)\hat{\boldsymbol{\imath}} + \frac{y}{r}\left(5\frac{z^2}{r^2}\right)\hat{\boldsymbol{\jmath}} + \frac{z}{r}\left(5\frac{z^2}{r^2}\right)\hat{\boldsymbol{k}}\right] \quad (2)$$

Where:

$\mathbf{P}_{J2}$ = perturbing acceleration vector

J_2 = J_2 zonal harmonic coefficient (0.00108263)

R = Earth equatorial radius (6378.137km)

r = Magnitude of the satellite's displacement

μ = GM (G = Gravitational constant, M = Mass of Earth)

x, y, z = satellite displacement along cartesian coordinate system axes

3.3.1 Alternative Oblateness Models

Although the J_2 perturbation model appears to be a very basic, a significant benefit of its implementation is computational speed and efficiency. As this project does not have access to an extensive amount of computational power, it is limited in complexity. In order to gain a non-trivial benefit in accuracy, a significant number of series terms must be included, due to the importance of the subsequent terms decreasing continuously, as the coefficients accompanying each term reduces by multiple orders of magnitude[18]. The implementation of more complex models, such as the "JGM-3" model, or the more complex "EGM96" model, increase computational requirements significantly, with the models containing 1,365[25], and 130,317[14] coefficients respectively.

3.4 Lunar Perturbation Model

The perturbing gravitational force from the Moon is approximated with Newton's law of gravitation where the Moon is assumed to be a point mass. Computing the positions across time of the body is more complex, since the Moon's orbital plane is inclined with respect to the Earth's equator, its position cannot be described by a simple repeatable equation. This dilemma is solved by considering a geocentric ecliptic reference frame, where the Sun, Moon and Earth all lie on the same orbital plane, this allows for computation of the Moon's position with simple repeating equations, which can be transformed to the equatorial reference frame for use in the model. The position is calculated using the known time at which the position is to be obtained. The process for calculating the Lunar position and the transform to the equatorial frame are shown below.

Alphabetic symbols a, b, c, d, e, f, g, and k, refer to numerical coefficients that can be found in table 1, and all angles calculated are wrapped to 360°.

First the Lunar ecliptic longitude(3) and latitude(4) are calculated[18].

$$\lambda_m = b_0 + c_0 T_0 + \sum_{i=1}^{6} a_i \sin(b_i + c_i T_0) \quad (3)$$

$$\delta_m = \sum_{i=1}^{4} d_i \sin(e_i + f_i T_0) \quad (4)$$

Where:

T_0 = Number of Julian centuries since J2000 (01/01/2000)

λ_m = Lunar ecliptic longitude

δ_m = Lunar ecliptic latitude

ε_m = Lunar obliquity to the ecliptic plane

The obliquity to the ecliptic plane(5) is then calculated[18].

$$\varepsilon_m = 23.439° - 0.0130042 T_0 \quad (5)$$

The horizontal parallax(7) is now computed[18], before the Moon's displacement magnitude(6). The figure 9 below shows how the horizontal parallax angle relates geometrically to the lunar displacement, this is possible as the system is being considered in the ecliptic plane, and can be flattened to 2 dimensions.

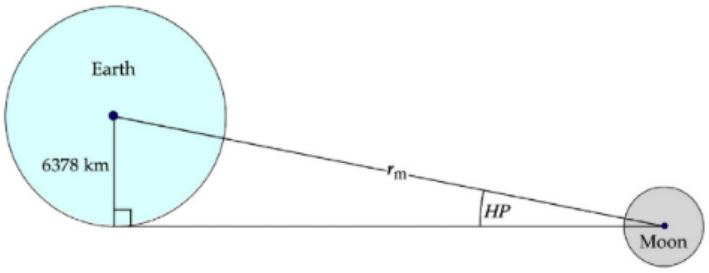

$$r_m = \frac{R}{\sin HP} \quad (6)$$

Figure 9 - Diagram showing the trigonometric relation of the Horizontal Parallax[18]

$$HP = g_0 + \sum_{i=1}^{4} g_i \cos(h_i + k_i T_0) \quad (7)$$

Finally, the geocentric lunar position vector(8) is calculated using the ecliptic longitude, latitude, and obliquity[18].

$$\boldsymbol{r}_m = r_m \cos\delta_m \cos\lambda_m \,\hat{\boldsymbol{\imath}} + r_m(\cos\varepsilon_m \cos\delta_m \sin\lambda_m - \sin\varepsilon_m \sin\delta_m)\hat{\boldsymbol{\jmath}} + r_m(\sin\varepsilon_m \cos\delta_m \sin\lambda_m + \cos\varepsilon_m \sin\delta_m)\hat{\boldsymbol{k}} \quad (8)$$

3.5 Solar Perturbation Model

The perturbing gravitational force of the Sun is computed with much similarity to the Lunar model, the solar gravity is described by Newton's point mass gravitational approximation. As the Sun's orbit is also inclined relative to Earth's equatorial plane, the calculation of the solar position uses a similar ecliptic-to-equatorial transformation method as before. This method of calculation and positional transformation is shown below.

The mean solar longitude(9), and mean solar anomaly(10) are calculated[18].

$$L_s = 280.459° + 0.98564736°n \quad (9)$$

$$M_s = 357.529° + 0.98560023°n \quad (10)$$

Where:

n = Number of Julian days since J2000

L_s = Mean solar longitude

M_s = Mean solar anomaly

λ_a = Apparent solar longitude

These values are used to compute the apparent solar longitude(11), as observed from Earth[18].

$$\lambda_a = L_s + 1.915° \sin M_s + 0.02° \sin 2M_s \quad (11)$$

The Sun's displacement magnitude(12) can now be computed using the mean anomaly[18].

$$r_s = (1.00014 - 0.01671 \cos M_s - 0.0014 \cos 2M_s)AU \quad (12)$$

The Sun's obliquity to the geocentric plane(13) is then calculated[18].

$$\varepsilon_s = 23.439 - 3.56 \times 10^{-7} n \quad (13)$$

Finally, the Solar position vector(14) can be calculated[18].

$$\hat{\boldsymbol{u}}_s = \cos\lambda_a \,\hat{\boldsymbol{\imath}} + \sin\lambda_a \cos\varepsilon_s \,\hat{\boldsymbol{\jmath}} + \sin\lambda_a \sin\varepsilon_s \,\hat{\boldsymbol{k}} \quad (14)$$

a	b	c	d	e	f	g	h	k
	218.32	481267.881				0.9508		
6.29	135	477198.87	5.13	93.9	483202.03	0.05	135	477198.87
-1.27	259.3	-413335.36	0.28	220.2	960400.89	0.0095	259.3	-413335.3
0.66	235.7	890534.22	-0.28	318.3	6003.15	0.0078	253.7	890534.22
0.21	269.9	954397.74	-0.17	217.6	-407332.2	0.0028	269.9	954397.7
-0.19	357.5	35999.05						
-0.11	106.5	966404.03						

Table 1 - List of coefficients for Luni/Solar positioning equations[18]

3.6 Radiation Pressure

Direct solar radiation pressure or “SRP” has been shown to have a non-trivial perturbing effect on satellites in MEO, in this project, SRP is modelled using the cannonball approximation, whereby the shape of the satellite is removed as a variable, being approximated as a reflective spherical mass or “cannonball”, leading to the effect of SRP being simplified to a single parameter, its area-to-mass ratio. This approximation is used to reduce computational cost, as accurate 3D modelling of SRP using techniques such as ray tracing is extremely computationally expensive and would give very little benefit to the accuracy of the results and require a large amount of additional research to create, which is beyond the scope of this project. The equation for the acceleration due to SRP(15) is given below[18]. While the solar constant, S, does in reality have some variation across time due to a number of phenomena such as sunspots and solar flares. This model assumes the value to be constant, as there is no definite pattern that can be described mathematically, and more importantly the effect of SRP is 3 orders of magnitude smaller than the perturbing effect of Earth’s oblateness, resulting in a negligible error due to this approximation.

$$\boldsymbol{a}_{srp} = -v\frac{S}{c}C_r A_{ratio}\hat{\boldsymbol{u}}_{srp} \tag{15}$$

Where:

$\mathbf{a}_{srp}$ = SRP perturbing acceleration vector

v = Shadow function (v = 0 or 1)

S = Solar constant (1367W/m^2)

c = Speed of light (299,792,000 m/s)

C_r = Coefficient of reflectivity (assumed to be 2)

A_{ratio} = Satellite’s area/mass ratio (m^2/kg)

$\mathbf{U}_{srp}$ = SRP direction vector

An additional method was added to the SRP model, in order to determine whether the satellite is in Earth’s shadow and subsequently being acted on by SRP, or not. Shown as the “Shadow function” in the equation above, this method works by constructing a line that passes through the position of the Sun and satellite, setting the equation of this line equal to the equation of a sphere with a radius equivalent to that of Earth’s equator, and solving for the discriminant of the resulting polynomial to determine if the line passes through the Earth and hence if the satellite is in Earth’s shadow.

4.0 Implementation

4.1 Numerical Integration Scheme

To solve the derived equations describing the motion of the satellite and all perturbing forces, a numerical integration scheme, implemented in MATLAB, was used. The integrator algorithm chosen to compute solutions for this model was MATLAB's own built-in ODE113 ordinary differential equation solver. This was chosen as it showed superior solution solve times over other available solvers like ODE23 or ODE45, and ODE113 is described as being "more efficient than ODE45 at problems with stringent error tolerances, or when the ODE function is expensive to evaluate"[26], two conditions present in this problem.

MATLAB's ODE113 solver is based on the Adams-Bashforth-Moulton numerical integration method, and uses a Predict-Evaluate-Correct-Evaluate (PECE) multistep algorithm to find solutions, while also incorporating a number of useful features that give the solver a very high level of accuracy alongside its impressively low computational cost. The solver features continuously variable step size and variable order up to an order of 13, while incorporating error checking at each timestep to allow the solver to adjust its step size and order of the solution in order to reach the required level of accuracy defined by the error tolerances chosen. Overall, ODE113 is a very robust and accurate integration method and is more than suitable for this use case.

The multistep PECE integration process of the Adams-Bashforth-Moulton method is as follows[27]:

1. The initial prediction step evaluates the values of the solution for the future timestep, using the given derivative equations that are to be numerically integrated, and only the values of the current state.

2. The first evaluation step calculates the error of the solution for comparison to the error tolerances set.

3. The corrector step considers and current state values, as well as the values from the 2 previous timesteps, using this information, the final future timestep solution predicted initially is tuned to reduce the overall error.

4. The final evaluation step calculates the error of the new tuned solution for comparison to the tolerances, to ensure that the solution is within the accepted level of accuracy.

4.2 Time Scheme

The concept of Julian days was used as the software implementations method of computing and recording date and time values, as well as the conversion method between the regular date format of DD/MM/YYYY. This quantity is defined as the number of days since January 1st 4713BC, a similar concept to UNIX time, and is used as the datum in this project. This allows the software

implementation to produce results with high accuracy in terms of the exact date and time at which the solution was computed.

4.3 Equation Modelling in MATLAB

Before the derived equations can be solved using the numerical integration scheme in MATLAB, some modification was done in order to compile them into a compatible form for software implementation. The modification and compilation steps are shown below.

First, equation 1 is divided through by the satellites mass, yielding the resulting acceleration on the satellite(16), the resulting equation is shown below, with the acceleration terms substituted for their appropriate variables mentioned in section 3.

$$\boldsymbol{a}_{sat} = \boldsymbol{a}_{Earth} + \boldsymbol{p}_{J2} + \boldsymbol{a}_{Sun} + \boldsymbol{a}_{Moon} + \boldsymbol{a}_{SRP} \tag{16}$$

The equations regarding the point mass gravitational approximation of the Sun(17), Moon(18), and Earth(19) can now be formulated, and are shown below.

$$\boldsymbol{a}_{Sun} = \frac{Gm_{Sun}}{r_s - r} \tag{17}$$

$$\boldsymbol{a}_{Moon} = \frac{Gm_{Moon}}{r_m - r} \tag{18}$$

$$\boldsymbol{a}_{Earth} = \frac{Gm_{Earth}}{r} \tag{19}$$

Where:

$\mathbf{a}_{Sun}$ = Acceleration due to solar gravity

$\mathbf{a}_{Moon}$ = Acceleration due to lunar gravity

$\mathbf{a}_{Earth}$ = Acceleration due to Earth's gravity

G = Gravitational constant

m_{Sun} = Mass of the Sun

m_{Moon} = Mass of the Moon

m_{Earth} = Mass of the Earth

r = Satellite displacement

r_s = Sun displacement (Equation 12)

r_m = Moon displacement (Equation 6)

MATLAB's ODE113 function accepts only 1st order ODE's for computation, as a result, equation 16 was split using the chain rule and vectorised. The result is a system of 6 1st order differential equations that describe the satellites acceleration and velocity. This allows the integrator to solve directly into state vectors of velocity and displacement for easy conversion to the system of orbital elements.

4.4 Initial Conditions

A wide range of initial conditions were propagated with the model to build a "map" of a satellite's orbital lifetime across the MEO region. To define the deorbited state of a satellite, the condition was set for an altitude of 400km, at this altitude the satellite is considered to have deorbited due to atmospheric drag and the simulation was ended. All simulations have a starting epoch of 01/01/2021 and were allowed to propagate for a maximum of 200 years. The error tolerances for the solver were set to 1e-11, for both the absolute and relative error tolerance for all orbits.

Orbital Element	Parameter Range	Parameter Step Size
Semimajor axis	25,000km – 30,000km	500km (11 steps)
Eccentricity	0.001 – 0.6	0.06 (11 steps)
Inclination	55° - 65°	2° (6 steps)
Ascending Node	0°, 90°	90° (2 steps)
Argument of Periapsis	0 for all	
True Anomaly	0 for all	
SRP Coefficient	0.015, 1m^2/kg	
Total number of Orbits	2,904	

Table 2 - List of all Initial conditions and Step sizes for the model

This range of initial conditions were chosen to focus on the current locations of the world's GNSS constellations, in order to find the most feasible disposal orbits that could be used to efficiently deorbit the constellations when they reach the end of their service life. To visualise the area of the study, figure 10 below shows the current orbital locations of the GNSS constellations, along with the discretised regions of observation detailed above, with respect to their semimajor axis, inclination, and eccentricity.

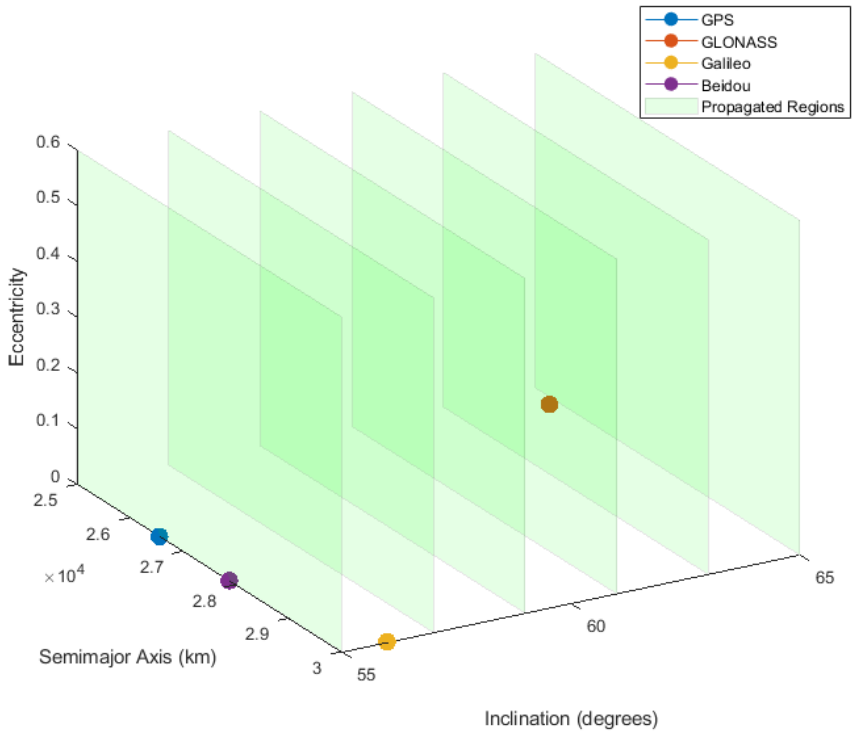

Figure 10 - Plot of GNSS Locations and Propagated Regions

4.5 Optimisation

Due to the large number of orbits propagated, and the computationally expensive model used, the software implementation was optimised as much as possible to decrease computation time. This was achieved by a variety of methods. Computational overhead was reduced by simplifying calculations as much as possible, as well as removing unnecessary variables and hardcoding constants and unchanging variables in for computational speed.

Due to the nature of numerical integration, it is impossible to parallelise the integration scheme across multiple cores, as each step of the solver requires the solution at the previous step to be known, confining the workload to a serialised flow. However, using MATLAB's Parallel Computing Toolbox, the workload of solving for each initial condition was split across multiple processing cores, allowing each core to compute results for a set of initial conditions. With this optimisation effort and the model running on a reasonably fast home machine (8 cores at 4.8GHz) the model completed the propagation of 2,904 orbits in approximately 60 hours, reduced from a previously unfeasibly long completion time.

This efficient model retains as much accuracy as possible, with the continuously changing lunar and solar positions as well as the SRP shadow function being updated and computed at each timestep of the integrator. The state vector solutions at every timestep from the model are saved at the end of each simulation, although only 1 in every 100 timestep solutions were actually saved as results, this was due to the file size becoming unmanageably large otherwise. However, this does not affect the accuracy of the results as this thesis is focussed on the orbital lifetime of the satellite, and is not concerned with the orbital state across time. Even with this reduction in file size, the resulting disk space occupied by all saved orbits was approximately 70GB. A flowchart of the computational method is shown below in figure 11, with the dotted lines representing the flow of calculated data between steps.

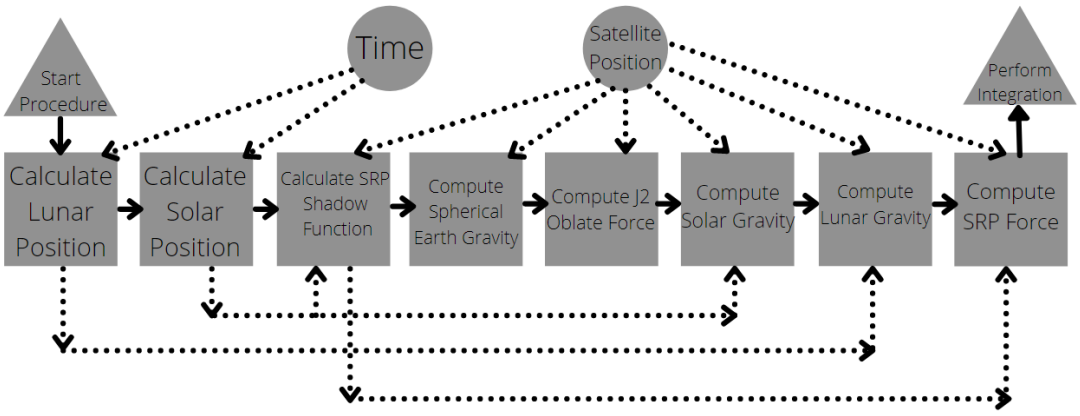

Figure 11 - Computational Method Flowchart

4.6 Validation of Results

To validate that the model was producing accurate solutions and was devoid of errors or software related bugs, a set of known results for a set of known initial conditions for the effects of each perturbation source, taken from the textbook “Orbital Mechanics for Engineering Students”[18], were used. The model was run with each individual perturbation source acting alone, in order to validate that each perturbing force was being modelled correctly. These validation simulations were carried out alongside the verified model supplied in the textbook, this model is denoted as the “control” on the figures below, and works in a similar manner, although it propagates the satellites position using a system of orbital elements as the variational parameters using the Gauss variational equations, rather than the displacement and velocity state vectors like in this paper. The results are comparable once the state vectors are converted to orbital element quantities. The table below shows the initial conditions used for each validation procedure of the perturbation sources.

The textbook only offers the source code of the model used, and the initial conditions alongside plots of the variation of the elements, it does not provide the direct numerical results from the simulations, therefore the verified model was run manually in order to generate the comparison figures.

Initial Conditions	**J2 Validation Value**	**SRP Validation Value**	**Lunar Validation Value**	**Solar Validation Value**
Semimajor axis	8,059km	10,085km	42,164km	6678.136
Eccentricity	0.17136	0.025422	0.0001	0.01
Inclination	28°	88.3924°	1°	28.5°
Ascending Node	45°	45.3812°	0°	0°
Argument of Periapsis	30°	227.493°	0°	0°
True Anomaly	40°	343.427°	0°	0°
Timespan	48 hours	3 years	60 days	60 days
Initial Epoch	01/01/2021	06/01/1964	01/07/2007	01/07/2007

Table 3 - Initial Conditions for Validation of the Model

4.6.1 J2 Perturbation Validation

The models were run with only the J2 perturbation active, and the variations of the eccentricity, inclination, and ascending node were compared to verify the accuracy and correctness of the model developed in this paper. The initial epoch for this procedure was chosen arbitrarily, as the J2 perturbation is not time dependant and is only a function of the satellite's position. The resulting comparison graphs are shown (figure 12, 13, 14) below, it can be clearly observed that the variation of the values match very closely in all cases, with very little deviation proving that the implementation of the J2 perturbation model was correct. The small discrepancy between the models could be explained by small differences in the values of constants used, and inherent computer arithmetic errors such as trying to subtract two nearly equal numbers, a well-documented characteristic that is caused by a computers finite level of decimal precision[28].

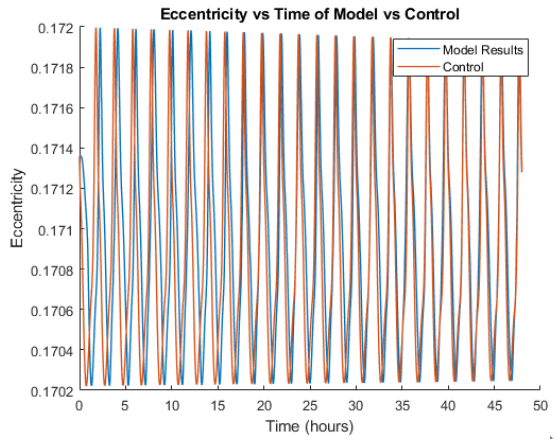

Figure 12 - Eccentricity plot for J2 Validation

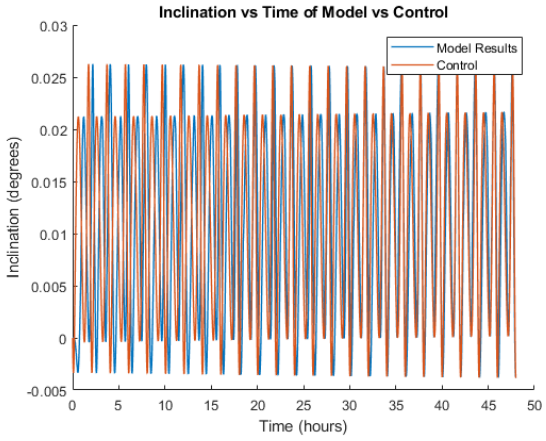

Figure 13 - Inclination plot for J2 Validation

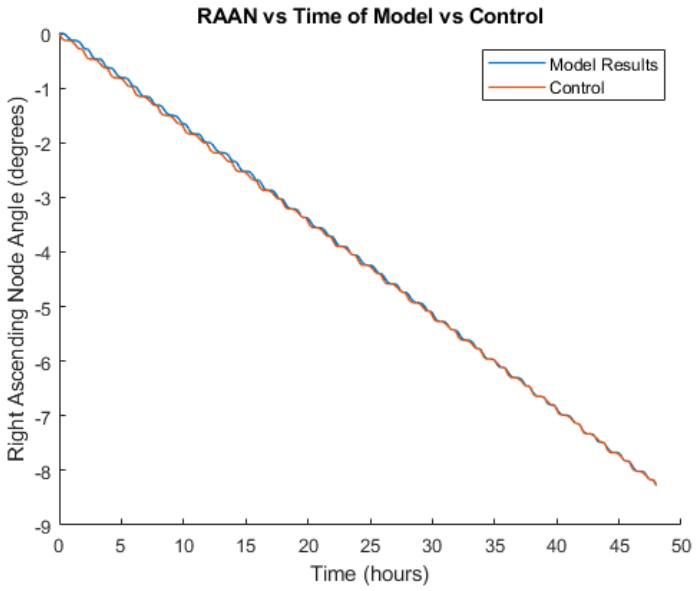

Figure 14 - Ascending Node plot for J2 Validation

4.6.2 SRP Perturbation Validation

The models were run with only the SRP perturbing force active with the initial conditions identical for both, and the variations of the eccentricity and ascending node were compared to validate the SRP model implementation. These figures (15, 16) are shown below, although there is some noticeable discrepancy between the variation of the elements, their general trend and shape is extremely similar, inferring that the SRP model is working as intended, the discrepancy may be explained due to a number of differences between the models, namely the error tolerances of the solver used, and the difference in solver method mentioned above, as well as the solver's initial step size. An area-to-mass ratio of $2m^2/kg$ were used for both models.

It is important to note that the verified control model used to validate the results is not a completely correct and accurate solution, it is simply a verified and trusted model that is comparable to the one developed in this paper. It is impossible to acquire a correct analytical solution that would be defined as the "right" answer.

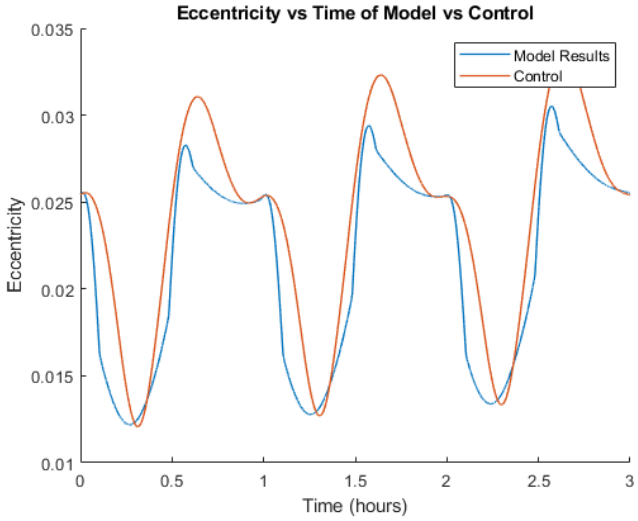

Figure 15 - Eccentricity plot for SRP Validation

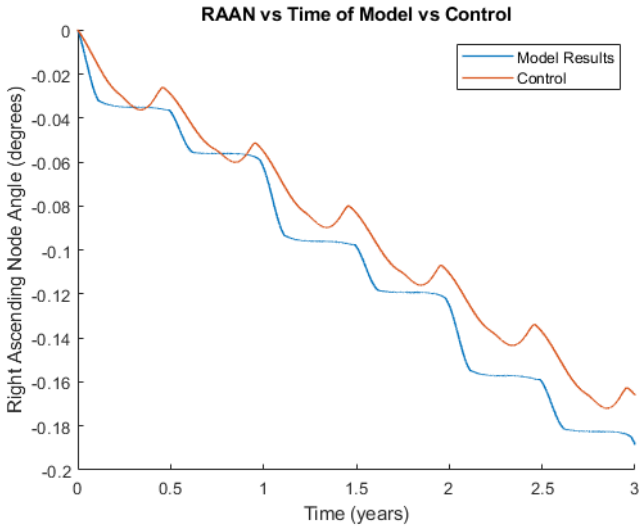

Figure 16 - Ascending node plot for SRP Validation

4.6.3 Lunar Gravity Perturbation Validation

The developed and control models were run again with only the lunar gravitational perturbation force active, using inclination and ascending node as the variational comparison values, shown below. It is clear that the lunar perturbation model is accurate, with the inclination plot (figure 17) showing identical shape in terms of variation across time, and the ascending node angle plot (figure 18) showing an exact inversion of the control models trend, this is due to a technicality concerning how and when angles are wrapped to 360° in the software implementation of the model. The difference between the control and test results present in the inclination values is again most likely caused by a difference in the model method.

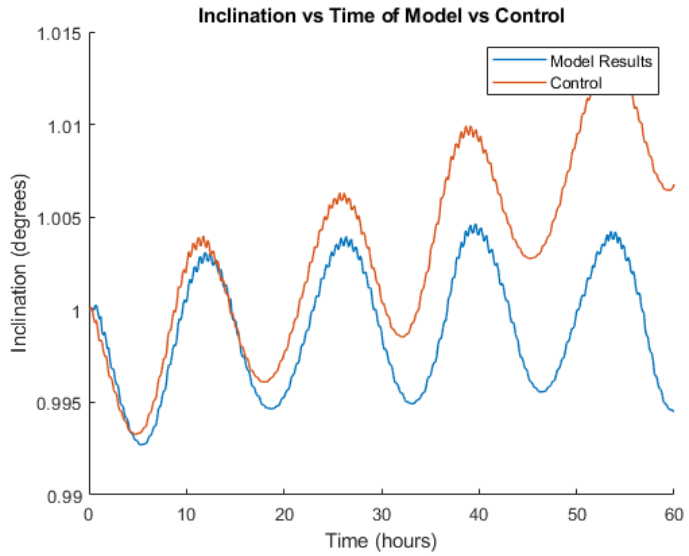

Figure 17 - Inclination plot for Lunar Validation

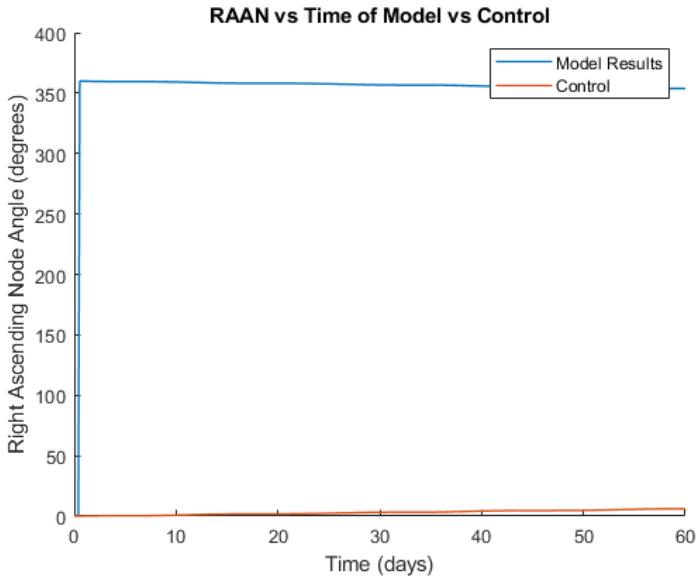

Figure 18 - Ascending node plot for Lunar Validation

4.6.4 Solar Gravity Perturbation Validation

As before, the developed and control models were run simultaneously but with only the solar gravitational perturbation active, and with inclination and ascending node as the variational comparison values, shown below. The solar perturbation model can be verified as accurate, as the ascending node plot (figure 20), neglecting the anomaly caused by angle wrapping, has an almost identical result to the control model, while the inclination plot (figure 19) appears to show an error, observing the magnitude of the scale on the Y-axis, shows very little relative difference between the models, this miniature discrepancy was most likely caused by differences in the model method once again.

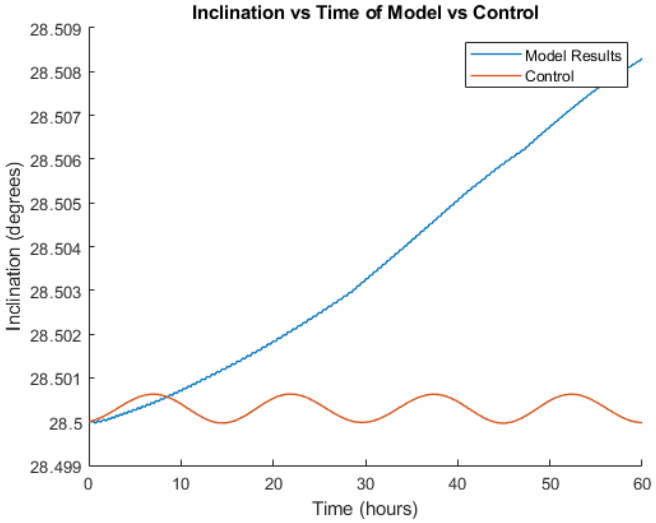

Figure 19 - Inclination plot for Solar Validation

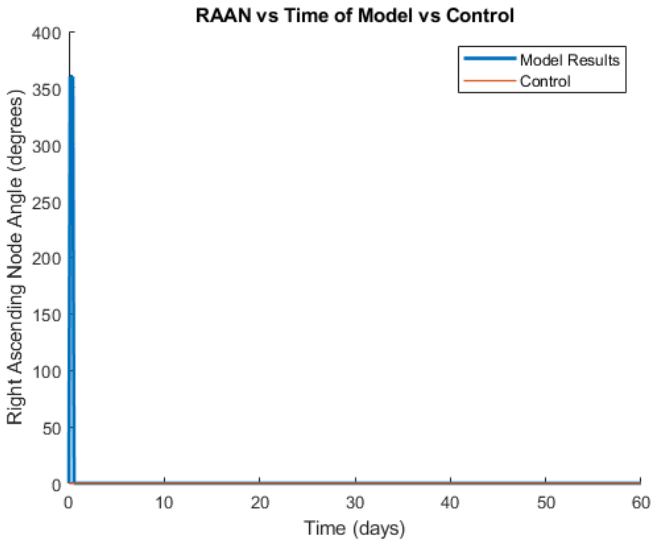

Figure 20 - Ascending node plot for Solar Validation

Overall, the model developed in this paper can be deemed as dynamically and mathematically accurate, with the verification results showing a clear likeness between the variation of different orbital parameters between the test model and control.

5.0 Discussion

5.1 Results

The acquired results are presented below in the form 2D colour maps of the propagated satellite's lifetime, with respect to its initial semimajor axis (X-axis), and eccentricity (Y-axis). Results are shown for each chosen angle of inclination, as well as the angle of ascending node, and each value of SRP coefficient.

5.1.1 Reading Disposal Orbit Feasibility from Results

Observing the results below, shows that there are a large number of orbits with short lifetimes spread across a wide range of orbital parameters. However, the vast majority possess a larger eccentricity, this paper aims to find disposal orbits for GNSS constellations, the orbits of which, possess eccentricity values very close to zero, making their orbits circular.

Just as the size of the manoeuvre a satellite can perform is defined by the amount of stored energy it possesses for use in changing its velocity, and hence its location. The feasibility of a disposal orbit can be defined by the amount of energy, or velocity, that is required by a satellite to transition onto it. This quantity is commonly known as "delta-v" (Δv), and is the difference in velocity the satellite must be able to achieve to transition to a desired orbit from its current one.

In relation to the circular nature of GNSS orbits, the amount of eccentricity that a satellite wishes to gain, is proportional to the value of delta-v that a satellite must achieve to complete that manoeuvre. Inferring that disposal orbits with lower eccentricities are more feasible as solutions for GNSS constellations. As satellites generally have little or no energy available for manoeuvres after they have reached their operating position, using disposal orbits with low delta-v requirements and low eccentricities is an ideal solution.

The results are plotted as described, due to the general relationship between delta-v size and type of manoeuvre required to change a satellites inclination, relative to changing its semimajor axis or eccentricity, it requires much more energy to alter the inclination compared to the other parameters. Therefore, the results are in their most useful form when representing semimajor axis and eccentricity.

In terms of numerical delta-v values, computation of this parameter requires defining much more specific design choices of the satellite in question, including the satellites mass, its thrust and manoeuvre capabilities, and its stored available energy. Therefore, evaluating the required delta-v values for specific GNSS satellites is beyond the scope of this paper.

As a reference for the delta-v requirements, a disposal orbit with eccentricity <0.3 is considered feasible in this paper, drawing from the suggestion of a similar study which used the same target value[10].

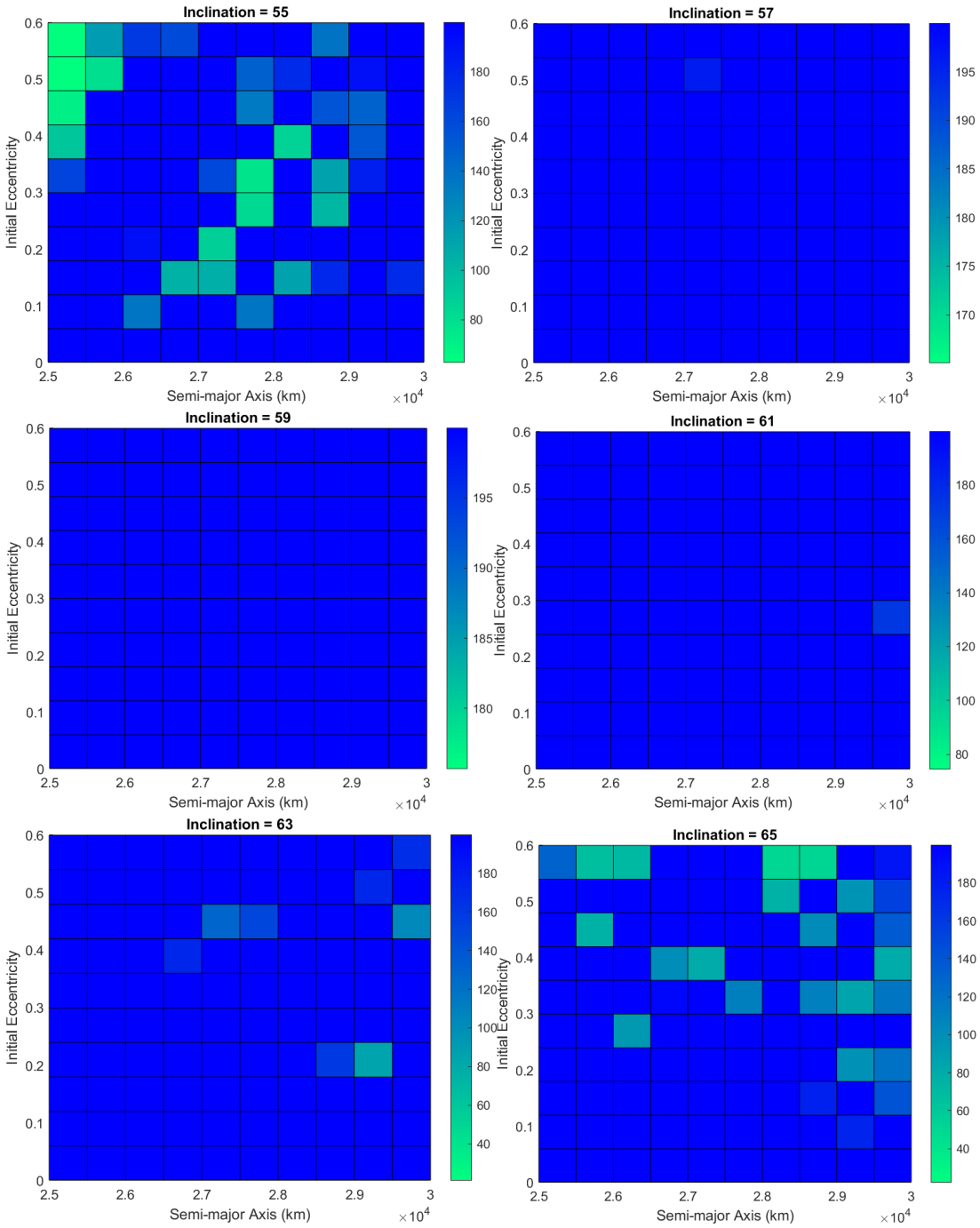

Figure 21 – Satellite Lifetime Results Map (A_{ratio} = 0.015m²/kg, Ascending node = 0°)

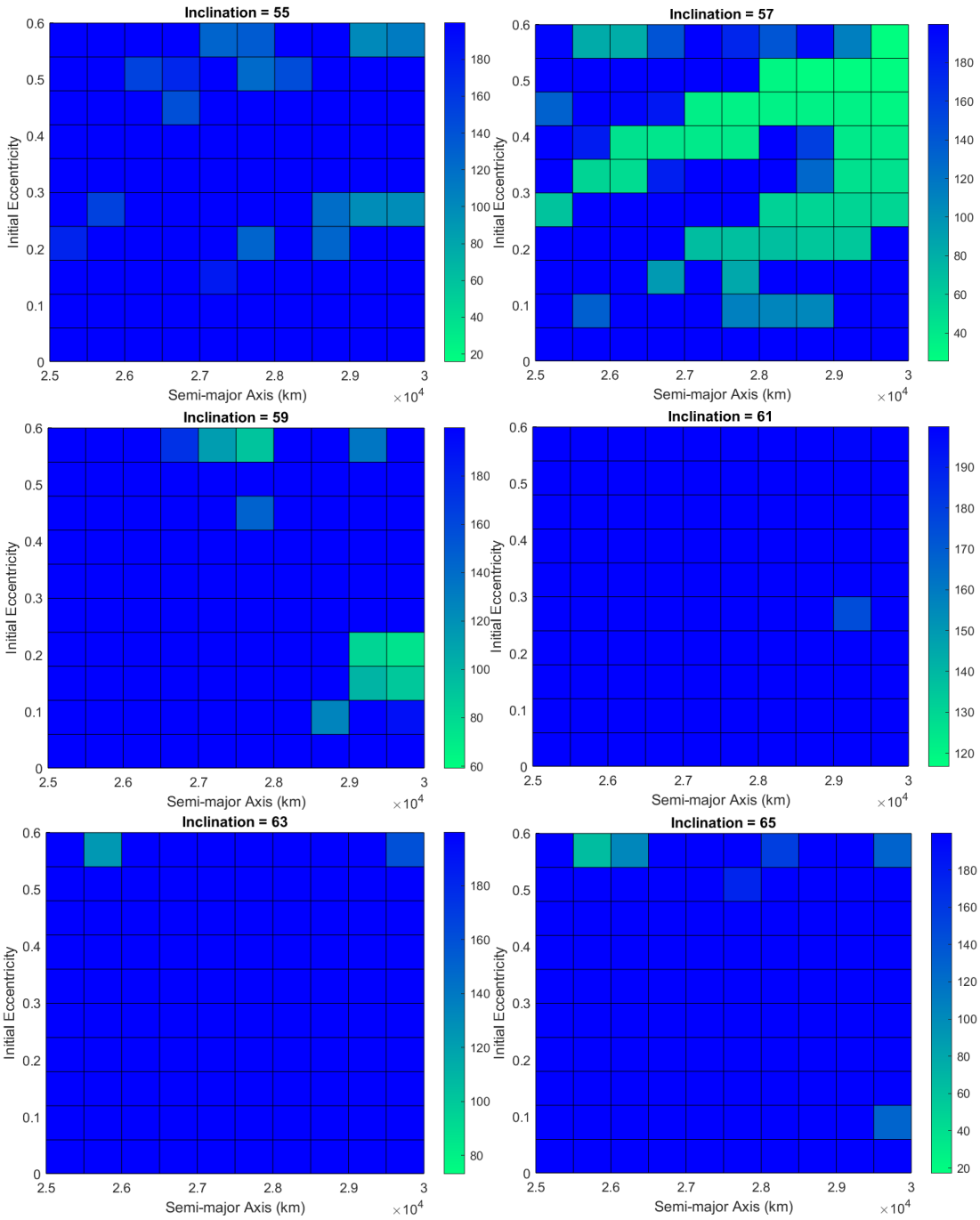

Figure 22 - Satellite Lifetime Results Map (A_{ratio} = 0.015m²/kg, Ascending node = 90°)

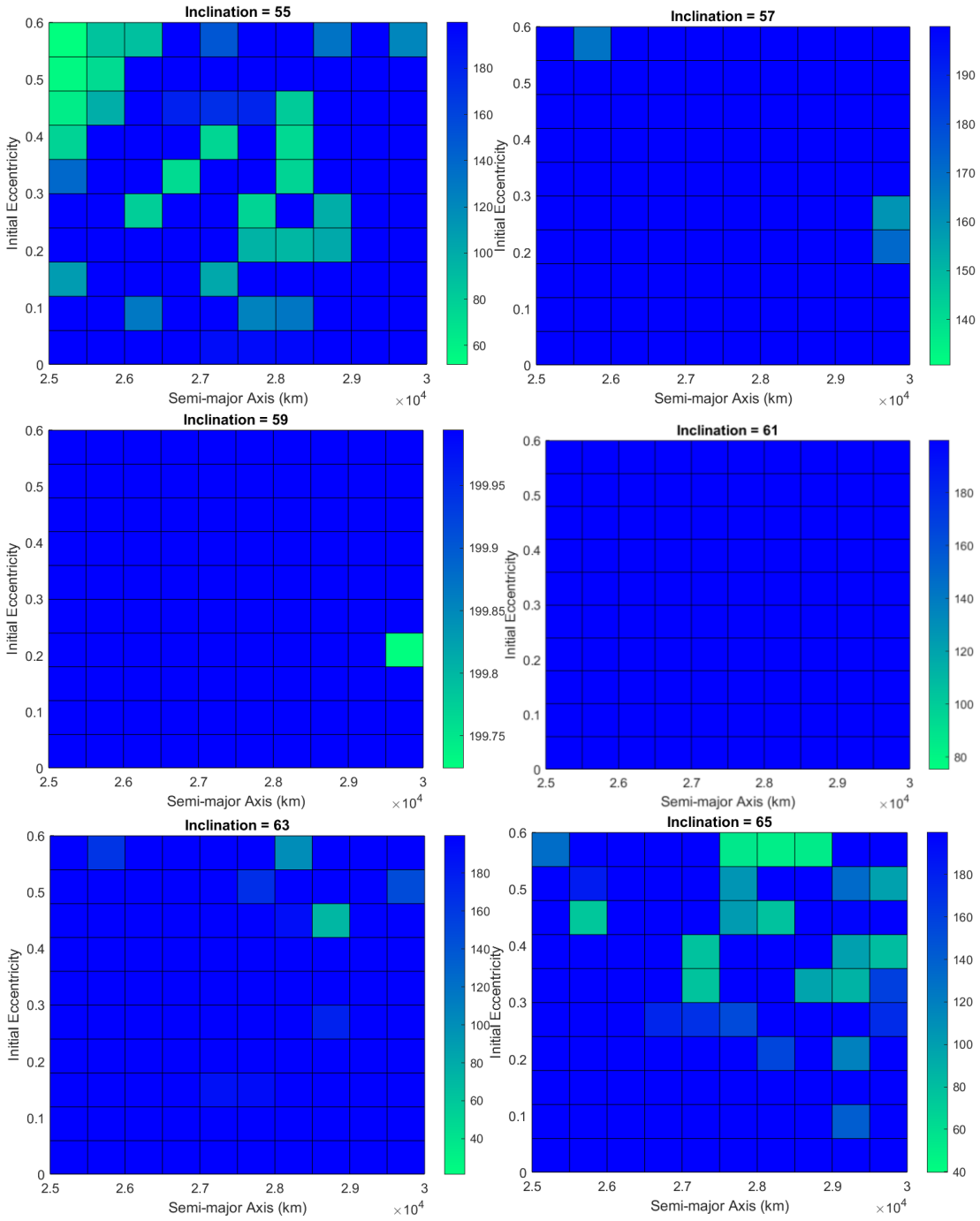

Figure 23 - Satellite Lifetime Results Map (A_{ratio} = 1m²/kg, Ascending node = 0°)

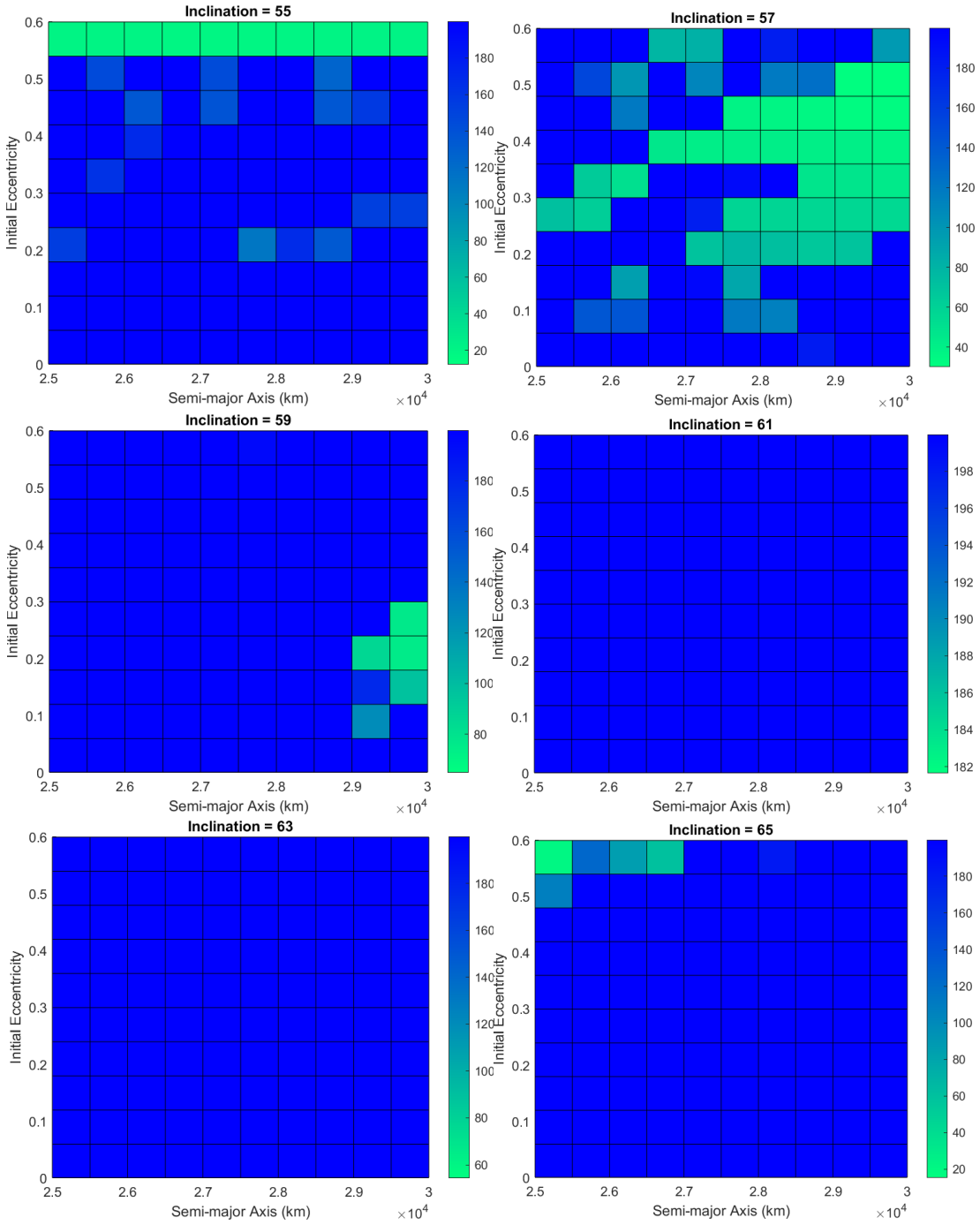

Figure 24 - Satellite Lifetime Results Map (A_{ratio} = 1m^2/kg, Ascending node = 90°)

5.1.2 Analysis of the Results

Considering the results as a whole, it is clear that the dynamical stability characteristics of the GNSS region are complex with no clear defining trend. However, specific conclusions can be drawn for subsections such as inclination and ascending node angle.

For an ascending node of 0 degrees, inclinations of 55 and 65 degrees (figure 21, 23) show many feasible disposal orbits with relatively low eccentricity, particularly in the case of 55 degrees inclination, where disposal orbits exist with lifetimes of less than 100 years, with eccentricities as low as 0.18. In contrast, the other values of inclination show regions of strong overall stability and long lifetime, with little to no visible disposal orbits, with the enhanced SRP coefficient retaining the same structure in the results.

In comparison to an ascending node of 90 degrees (figure 22, 24), the results are significantly different, with lower inclinations of 55, 57, and 59 degrees possessing the majority of feasible disposal orbits with low eccentricities. With an inclination of 57 degrees showing a large region of instability, occupied by disposal orbits with very short lifetimes of 100 to as low as 60 years. Higher inclinations, show regions of general stability, with no disposal orbits present at feasible eccentricities. These clusters of disposal orbits also appear to be independent of SRP coefficient, showing the same structure across both sets of results.

Even for values of lower area-to-mass ratio, disposal orbits are present throughout the results, at feasible values of eccentricity, with the enhanced SRP value showing the expected effect, adding instability while retaining the same overall trends across different inclinations. This effect is particularly visible at an inclination of 55 degrees and ascending node of 90 degrees (figure 24), where the enhanced SRP value has created a large region of instability at high eccentricities, independent of semimajor axis, where none was present in the low SRP results.

Some regions, like those with an inclination of 61 and 63 degrees, show little to no feasible disposal orbits, as a result of the complex lunisolar resonance harmonics, although the regions cannot be ruled out completely without reinvestigation at a higher resolution.

The variation of the ascending node shows a clear and significant change in the patterns of the results, inferring that the effects of the perturbing forces are strongly dependent on the initial angular orientation. It is also clear that variation of the inclination will result in radically different perturbing effects, with each value subject to its own dynamical complexities.

The semimajor axis appears to have no clear trend across the studied regions, suggesting that the perturbing effects have a much larger dependence on angular position rather than linear displacement. A very loose trend showing the majority of short lifetime orbits possess a higher semimajor axis, particularly at an inclination of 57 degrees, and ascending node of 90 (figure 22, 24), can be observed, however this is not significant enough to be drawn

as a conclusion. This unique property further confirms the idea that the perturbing forces depend most significantly on angular orientation, as variation of the semimajor axis only results in a change of linear displacement, with no angular alteration.

5.2 Limitations

Various limitation factors contributed to the quality of the results shown in this paper, these limitations are discussed below.

5.2.1 Limited Simulation Range

Due to the timeframe over which this project was completed, it was only possible to run simulations for a limited range of initial conditions, given more time, more simulations could be carried out to expand the range of results, allowing for the possible discovery of more disposal orbits. Furthermore, with access to a machine with a very large amount of computational power, such as a server farm or supercomputer, the resolution of the orbital lifetime maps could be increased also, allowing for higher accuracy regarding the exact locations of the disposal orbits, as the developed model is fully capable of scaling out across an increased number of processing cores.

5.2.2 Project Hindrances

During the very late stages of the project, a human error in the software implementation in MATLAB was discovered relating to the calculation of the Moon's position. This was discovered after several days had been spent propagating 10,584 orbits. As a result, these previous simulations were rendered useless as they were inaccurate. In order to complete this project within the given deadline, the resolution of the semimajor axis, and eccentricity steps, had to be reduced from 21 to 11, as shown in the table of initial conditions for the model, giving results of lower resolution.

Comparison of the resolution of the previously computed results, shows the enhanced ability to find disposal orbits, and the overall higher quality of the results. An example of this is shown below (figure 25), taken from a sample of the defunct set of data. This error has unfortunately hindered the quality of the results produced in this paper due to the loss of available computation time.

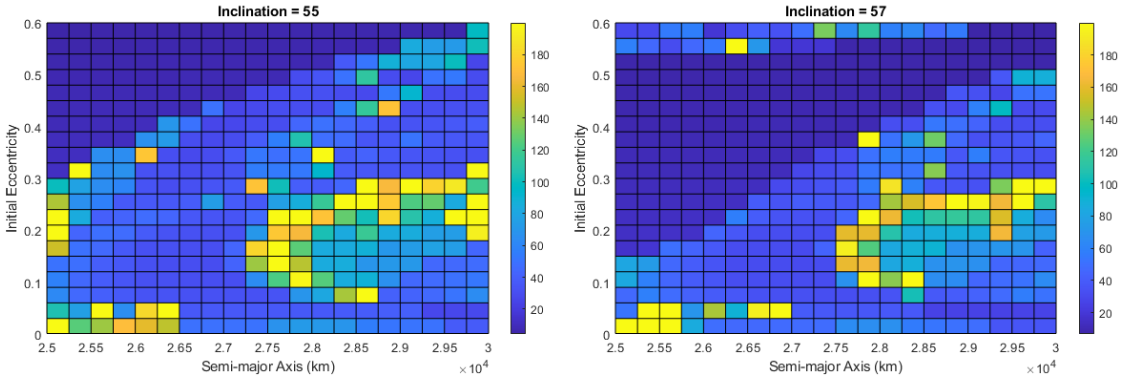

Figure 25 - Defunct Results Plot of Higher Resolution

(Inclination = 55° & 57°, A_{ratio} = 0.015m²/kg, Ascending Node = 90°)

6.0 Conclusions

This paper aimed to investigate the orbital lifetime of satellites in the GNSS sector of the MEO orbital region, in order to find feasible disposal orbits for space debris mitigation once the current GNSS satellite constellations reach end-of life, and evaluate some of the complex dynamical characteristics present as a result of various perturbations and resonances. The conclusions found are as follows.

- The results show that the GNSS and MEO region possess a vast array of distinct regions of inherent instability and eccentricity growth, with a spread of dynamical complexities overall.

- For an ascending node 0 at inclinations of 55 and 65 degrees, the results show many feasible disposal orbits, similarly for an ascending node of 90 degrees, lower inclinations of 55, 57, and 59, degrees show feasible orbits throughout.

- An inclination of 57 degrees at an ascending node angle of 90, shows a particularly interesting region, of a large cluster of instability from high to low eccentricity, with very short lifetimes of 100 to as low as 60 years.

- Higher angles of inclination for an ascending node of 90 degrees show stability overall, However, for an ascending node of 0 degrees, the centre angles of inclination (57-63 degrees) show the same pattern of stability with these patterns being independent of SRP coefficient.

- The SRP coefficient has no effect on the overall structure of the results, rather it shows an amplification effect, causing orbits of inherent instability to deorbit within a shorter time span, as well as inducing a faint level of instability overall.

- There are some regions that possess inherent stability, independent of SRP coefficient, and ascending node, these regions were located at inclinations of 61 and 63 degrees.

- The resulting effect from the perturbing forces appears to depend strongly on angular orientation, with the small variation of the ascending node and inclination producing a wide variation of different patterns with no likeness or common structure between them.

- The effects of the perturbing forces show almost no correlation to the linear displacement, categorised as the variation of the semimajor axis, with no clear trend presented by the results.

- Overall, a passive deorbiting strategy appears to be both economically and technically feasible for satellites in the current GNSS region, with a wide range of disposal orbits found with low eccentricities and for both values of SRP coefficient, across a wide range of initial conditions.

6.1 Further Work

Various concepts and ideas are discussed below concerning further work that would both improve and expand on the results presented, and dynamical model developed in this paper.

6.1.1 Expansion of Simulation Range

As mentioned previously, this paper covers only a small range of the MEO region related to current GNSS constellations, this range could be expanded to cover a far wider range of initial conditions, to evaluate the dynamical complexities across the entire MEO region, as well as the GEO region, which is home to a large number of satellites and debris.

In addition, many more orbital parameters could be varied, such as the argument of periapsis, a variable kept constant in this problem, which would allow for further insight into the dynamical trends of the region, furthermore, the resolution of the constructed maps, should be increased to allow for more confidence in the results and to locate more specific regions of disposal orbits.

6.1.2 Comparison of Different Model Methods

While the model in this paper uses the equations of motion describing the satellite to propagate its position, many other methods exist that can achieve this, such as the Gauss variational planetary equations, or the Hamiltonian equations. These methods could be compared in terms of computational efficiency as well as accuracy, to determine the optimal method for a given use case. In addition, the results of the propagation could be compared to real-world observations from observatory telescopes, to determine their absolute accuracy.

6.1.3 Adding Additional Functionality

The model developed in this project already possesses a high level of robustness and universal functionality, in that it is capable of propagating any orbit given any set of initial conditions, for any chosen timespan, and for any chosen initial starting epoch. However, as discussed previously, the magnitude of the perturbing forces varies depending on the orbital region being investigated, for example, aerodynamic drag being most significant at only very low altitudes. To expand the functionality of the model further, suitable models for all perturbing forces present across different orbital regions could be implemented, as currently this model is most accurate when simulating in the MEO region.

For additional accuracy in the results, adjustments to the lunar perturbation model could be made, with the inclusion of the Moon's libration cycles, similarly, the solar constant, present in the SRP approximation, could be more accurately modelled as a function of distance, rather than being assumed constant.

7.0 Acknowledgements

I would like thank my project supervisor and mentor, Dr Jinglang Feng, for continuous support, advice, and knowledge throughout the completion of this project. I could not have asked for a more punctual and helpful mentor, to guide me through my first full-scale academic paper.

I would also like to thank my close family and friends for their emotional support throughout this unprecedented and stressful time.

8.0 References

[1] European_Space_Agency, “About Space Debris.” https://www.esa.int/Safety_Security/Space_Debris/About_space_debris (accessed Jan. 27, 2021).

[2] M. Mejía-Kaiser, “IADC Space Debris Mitigation Guidelines,” *Geostationary Ring*, pp. 381–389, 2020, doi: 10.1163/9789004411029_014.

[3] “GNSS | GEOG 862: GPS and GNSS for Geospatial Professionals.” [Online]. Available: https://www.e-education.psu.edu/geog862/node/1871.

[4] E. M. Alessi *et al.*, “Effectiveness of gnss disposal strategies,” *Proc. Int. Astronaut. Congr. IAC*, vol. 3, pp. 2047–2060, 2013.

[5] SpaceDaily, “Soyuz launch from Kourou postponed until 2021,” 2020. https://www.spacedaily.com/reports/Soyuz_launch_from_Kourou_postponed_until_2021_2_others_to_proceed_999.html (accessed Apr. 09, 2020).

[6] N. L. Johnson, “Medium earth orbits: is there a need for a third protected region?,” *61st Int. Astronaut. Congr. 2010, IAC 2010*, vol. 7, pp. 5594–5600, 2010.

[7] “ClearSpace-1: Earth’s First Space Debris Removal Mission.” [Online]. Available: https://scitechdaily.com/clearspace-1-earths-first-space-debris-removal-mission/.

[8] M. M. Castronuovon, “Active space debris removal-A preliminary mission analysis and design,” *Acta Astronaut.*, vol. 69, no. 9–10, pp. 848–859, 2011, doi: 10.1016/j.actaastro.2011.04.017.

[9] E. M. Alessi *et al.*, “A numerical investigation on the eccentricity growth of GNSS disposal orbits,” *Celest. Mech. Dyn. Astron.*, vol. 125, no. 1, pp. 71–90, 2016, doi: 10.1007/s10569-016-9673-4.

[10] D. K. Skoulidou, A. J. Rosengren, K. Tsiganis, and G. Voyatzis, “Medium Earth Orbit dynamical survey and its use in passive debris removal,” *Adv. Sp. Res.*, vol. 63, no. 11, pp. 3646–3674, 2019, doi: 10.1016/j.asr.2019.02.015.

[11] A. B. Jenkin, M. E. Sorge, J. P. Mcvey, G. E. Peterson, and B. Y. Yoo, “Meo debris environment projection study,” *6th Eur. Conf. Sp. Debris*, vol. 2013, no. April, pp. 22–25, 2013, [Online]. Available: http://articles.adsabs.harvard.edu/cgi-bin/nph-iarticle_query?2013ESASP.723E..40J&data_type=PDF_HIGH&whole_paper=YES&type=PRINTER&filetype=.pdf.

[12] T. Reid, “Orbital Diversity for Global Navigation Satellite Systems,” 2017.

[13] P. M. Sforza, “Chapter 5 - Orbital Mechanics,” in *Manned Spacecraft Design Principles*, P. M. Sforza, Ed. Boston: Butterworth-Heinemann, 2016, pp. 75–115.

[14] R. H. R. and T. R. O. F. G. Lemoine, S. C. Kenyon, J. K. Factor, R.G. Trimmer, N. K. Pavlis, D. S. Chinn, C. M. Cox, S. M. Klosko, S. B. Luthcke, M. H. Torrence, Y. M. Wang, R. G. Williamson, E. C. Pavlis, "The Development of the Joint NASA GSFC and the National Imagery and Mapping Agency (NIMA) Geopotential Model EGM96," 1998.

[15] S. Breiter, "Lunisolar Resonances Revisited," *Celest. Mech. Dyn. Astron.*, vol. 81, 2001, doi: 10.1023/A:1013363221377.

[16] J. Radtke, R. Domínguez-González, S. K. Flegel, N. Sánchez-Ortiz, and K. Merz, "Impact of eccentricity build-up and graveyard disposal Strategies on MEO navigation constellations," *Adv. Sp. Res.*, vol. 56, no. 11, pp. 2626–2644, 2015, doi: 10.1016/j.asr.2015.10.015.

[17] D. K. Skoulidou, A. J. Rosengren, K. Tsiganis, and G. Voyatzis, "Cartographic Study of the Meo Phase Space for Passive Debris Removal," *7th Eur. Conf. Sp. Debris*, no. April, pp. 18–21, 2017.

[18] H. D. Curtis, "Introduction to Orbital Perturbations," in *Orbital Mechanics for Engineering Students*, 2014, pp. 651–720.

[19] J. Daquin, A. J. Rosengren, E. M. Alessi, F. Deleflie, G. B. Valsecchi, and A. Rossi, "The dynamical structure of the MEO region: long-term stability, chaos, and transport," *Celest. Mech. Dyn. Astron.*, vol. 124, no. 4, pp. 335–366, 2016, doi: 10.1007/s10569-015-9665-9.

[20] K. Bugs, F. Tests, O. Findings, T. Procedures, E. Tests, and R. A. Tests, "Spec User ' s Guide."

[21] Wikipedia, "FreeFlyer." https://en.wikipedia.org/wiki/FreeFlyer.

[22] A.I.-Solutions, "Choosing an Integrator." https://ai-solutions.com/_help_Files/choosing_an_integrator.htm.

[23] AGI, "AGI STK." that enables engineers and scientists to perform complex analyses of ground, sea, air, and space platforms.

[24] Wikipedia, "Orbital Elements." https://en.wikipedia.org/wiki/Orbital_elements.

[25] B. D. Tapley *et al.*, "The Joint Gravity Model 3," *J. Geophys. Res. Solid Earth*, vol. 101, no. B12, pp. 28029–28049, 1996, doi: https://doi.org/10.1029/96JB01645.

[26] Mathworks, "Choose an ODE Solver - MATLAB," *Mathworks MATLAB Help Center*. https://uk.mathworks.com/help/matlab/math/choose-an-ode-solver.html.

[27] R. R. Bate, D. D. Mueller, and J. E. White, *Fundamentals of Astrodynamics*. Dover Publications, 1971.

[28] "Five Tips for Floating Point Programming - CodeProject." [Online]. Available: https://www.codeproject.com/articles/29637/five-tips-for-floating-point-programming.

DEPARTMENT OF MECHANICAL & AEROSPACE ENGINEERING

University of Strathclyde Engineering

Technical Paper

Class Code/ Title:	ME420 / Individual Project - Aerospace
Technical paper title:	Investigation of the orbital lifetime of GNSS satellites in the MEO region with a numerical integration orbit propagation model.
Student Name/ Number:	Jacob Currie / 201718558
Supervisor:	Dr. Jinglang Feng
Date:	04/03/2021
Word count:	2953

Abstract

With space debris becoming an increasingly more significant problem as technological advances in the space industry push us closer to a space-conquering society, the importance of the MEO space region is increasing for GNSS satellite constellations, leading to more debris in this previously sparsely populated region. The aim of this paper is to investigate the dynamics of satellites in orbits similar to current GNSS systems, and using a mathematical model developed from this, predict the orbital lifetime of the satellites and evaluate the feasibility of a deorbit manoeuvre for GNSS satellites reaching end-of-life, in order to mitigate possible debris. This paper details the development of the model, along with its implementation in MATLAB R2020b, a discussion of the acquired results as well as further recommendations for continued work and improvement.

Contents

Nomenclature

Bold letters are representative of vectors

Symbol	Description	Units
A_{ratio}	Satellite area to mass ratio	m^2/kg
$\mathbf{a}_{srp}$	SRP perturbing acceleration vector	km
c	Speed of light	m/s
C_r	Coefficient of Reflectivity	
F_{Earth}	Earth's Gravitational force	N
F_{J2}	J2 perturbing force	N
F_{Moon}	Moon's Gravitational force	N
F_{sat}	Net force acting on the satellite	N
F_{SRP}	Solar Radiation Pressure force	N
F_{Sun}	Sun's Gravitational force	N
HP	Lunar horizontal parallax	°
J_2	J_2 zonal harmonic coefficient	
L_s	Mean solar longitude	°
M_s	Mean solar anomaly	°
n	Number of Julian days after J2000	
$\mathbf{P}_{J2}$	Perturbing acceleration from J_2	km^2/s
r	Satellite displacement magnitude	km
R	Earth's equatorial radius	km
$\mathbf{r}_m$	Moon position vector	km
$\mathbf{r}_s$	Sun position vector	km
S	Solar Constant	W/m^2
T_0	Number of Julian centuries after J2000	
$\mathbf{u}_{srp}$	Sun-to-Satellite direction vector	km
v	Shadow function	
δ	Lunar ecliptic latitude	°
ε_m	Lunar obliquity to the ecliptic plane	°
ε_s	Solar obliquity to the ecliptic plane	°
λ	Lunar ecliptic longitude	°
λ_a	Apparent solar longitude	°

1.0 Introduction

In order to investigate and analyse the stability and lifetime of a satellite's orbit, it must be propagated using an accurate mathematical model that approximates the dynamics and forces acting on an object in orbit. This is achieved by deriving the equations that describe the motion of a satellite as it is acted on by various gravitational and perturbing forces, these equations are used to simulate the satellite's orbital state across time using numerical integration.

1.1 Literature Review

As space debris becomes an increasingly dangerous and important threat to satellites in service in the MEO region, it is clear that something must be done to mitigate the build-up of space junk and avoid reaching the levels already currently present in the LEO and GEO regions. Space debris poses a threat of collision and damage to operational satellites, and in the event of this occurring, will further increase the risk of collision with more objects, as the amount of debris is increased with each collision. The threat increases in size as time passes, as the amount of debris has been steadily increasing, reaching over 1000 tracked objects in MEO in 1992[1]. Even with the vast majority of debris being present in the LEO region, a significant amount is also found across the MEO region, most notably at altitudes of 2000km and 20,000km[1].

The world's GNSS (Global Navigation Satellite System) constellations, namely GPS, GLONASS, Galileo, and Beidou, operate in the MEO region at altitudes between 25,000km and 30,000km, on inclined orbits around 55° to 65°, where a large number of non-operational satellites categorised as debris also reside. With humanity's push towards being a space-conquering civilisation, it is increasingly clear that space debris mitigation strategies are important to realising this goal.

Many previous papers have been written on this topic, investigating the orbital lifetime of satellites and the feasibility of re-entry manoeuvres. The relationship between orbital position and state, and the stable lifetime of the object in question, has been shown to be complex due to perturbations from Earth's oblateness, and the gravitational effect of the Sun and Moon[2]. The combination of these effects leads to complex, seemingly random orbital lifetimes at high inclinations[2]. While the perturbing effect of solar radiation pressure is shown to modify and enhance the re-entry characteristics of certain orbital conditions[2]. There are some noticeable trends in the relationship between orbital lifetime and the orbital state, such as a decrease in stability with respect to increasing eccentricity and inclination[3].

2.0 Mathematical Model

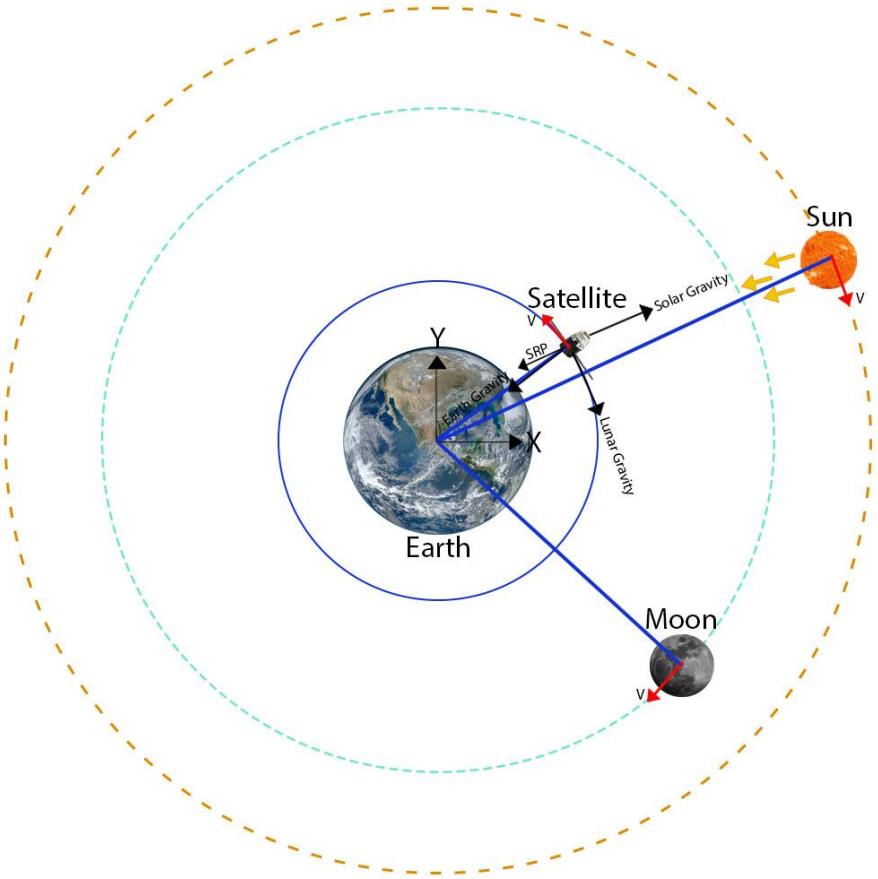

Figure 26 - Free body Diagram of Satellite and Orbit System

The equations of motion describing the satellite are derived from Newtons 2nd Law and Newtons law of gravitation, using a geocentric inertial reference frame, with the Z-axis defined as the Earth's polar axis, X-axis at 0° longitude (Greenwich), and Y-axis at 90° at the initial starting epoch of the model. Neglecting air resistance, and taking into account the gravitational forces of the Earth, Moon, and Sun, as well as direct solar radiation pressure (SRP), a free body diagram is shown in figure 1, taking forces around the satellite. The resulting equation from the free body diagram is shown below.

$$\sum F_{sat} = F_{Earth} + F_{J2} + F_{Sun} + F_{Moon} + F_{SRP} \quad (20)$$

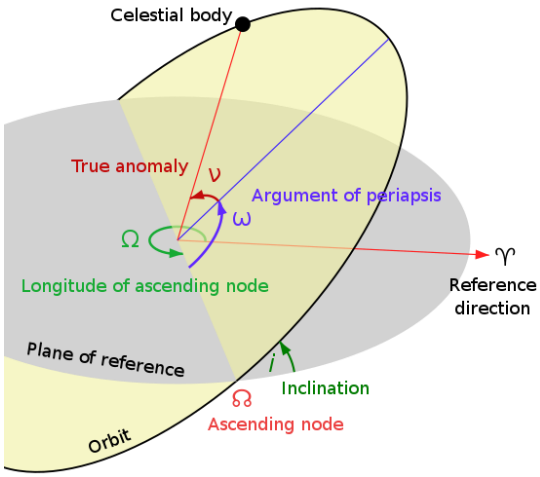

Figure 27 - Coordinate system diagram of Orbital Elements

To fully define and easily interpret a satellite's orbit, the system of 6 orbital elements, devised by Kepler, are used. These parameters can be used to convert between a cartesian coordinate system, more specifically, they can generate “state vectors”, which are two vector quantities describing the satellite's position and velocity, which also fully define its orbital state. These elements are defined as follows.

Semimajor axis, the distance between the furthest point of the orbit and the centre of the orbital ellipse.

Eccentricity, a measure of how circular or elliptical an orbit is.

Inclination, the angle at which the orbital plane is inclined from the reference plane.

Longitude of the ascending node, the angle measured around an axis normal to the reference plane, to the point where the orbital path crosses through the reference plane. This point is known as the ascending node.

Argument of periapsis, the angle measured in the orbital plane, between the reference plane and the point of periapsis (the point at which the satellite is closest).

True anomaly, the angle measured between the periapsis line and the point at which the satellite is currently positions along its orbit.

2.1 Oblate Spheroid Earth Model

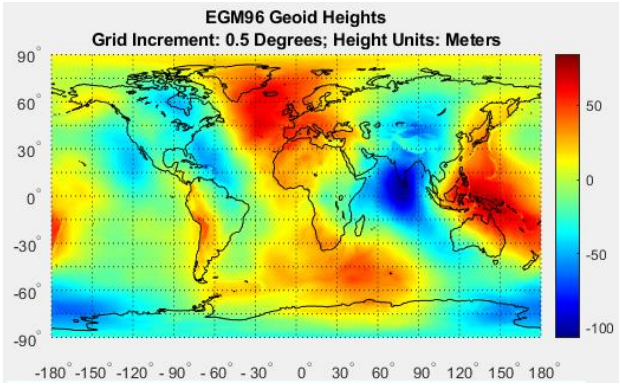

Figure 28 - Visualisation of Earth's Geopotential variation[4]

In order to accurately model the effect of Earth's gravity taking into account its oblateness, a special perturbation is added as a modifier to Newton's spherical approximation of Earth's gravity, that approximates the perturbing force on the satellite due to this geopotential variation, in this model the "J_2" perturbation is used, which approximates the perturbation force of a rotationally symmetric oblate mass, the equation for this, is given by an infinite series, however the most significant term by 3 orders of magnitude is the term J_2, it is generally accepted that term alone can be used as an approximation and is used in this case. The equation for the perturbing acceleration acting on the satellite is given below.

$$\boldsymbol{p}_{J2} = \frac{3}{2}\frac{J_2 \mu R^2}{r^4}\left[\frac{x}{r}\left(5\frac{z^2}{r^2}\right)\hat{\boldsymbol{\imath}} + \frac{y}{r}\left(5\frac{z^2}{r^2}\right)\hat{\boldsymbol{\jmath}} + \frac{z}{r}\left(5\frac{z^2}{r^2}\right)\hat{\boldsymbol{k}}\right] \quad (21)$$

Where:

P = perturbing acceleration vector

J_2 = J_2 zonal harmonic coefficient

R = Earth equatorial radius

r = Magnitude of the satellite's displacement

μ = GM (G = Gravitational constant, M = Mass of Earth)

x, y, z = satellite displacement along cartesian coordinate system axes

2.2 Lunar/Solar Gravitational Perturbations

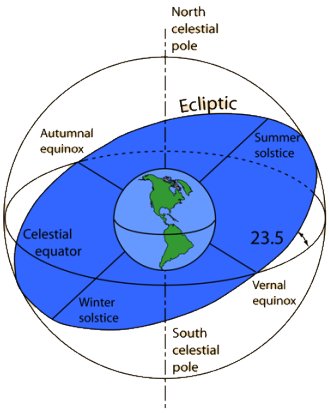

Figure 29 - Earth shown with Equatorial and Ecliptic planes[5]

In this model, the gravitational force from the Sun and Moon are approximated using Newton's law of gravitation for point masses, allowing for a simple mathematical approximation. Computing the positions across time of the perturbing bodies are more complex, since the orbits of the Earth, Sun, and Moon do lot lie on the same plane, the positions of the Sun and Moon relative to a geocentric equatorial reference frame cannot be simply defined with a repeatable equation. However, this dilemma can be solved by first considering the orbits of the Sun and Moon with respect to a geocentric ecliptic reference frame, in this frame the orbits can be defined easily, and transformed to the equatorial reference frame for use in the model. This is done using the known time at which the position is to be obtained, to calculate at what point along its orbit the body is located. The process for calculating the position of the Moon for a geocentric reference frame requires the computation of various other parameters, listed below[6].

Alphabetic symbols a, b, c, d, e, f, g, and k, refer to numerical coefficients that can be found in table 1, and all angles calculated are wrapped to 360°.

The Lunar ecliptic longitude and latitude are calculated.

$$\lambda = b_0 + c_0 T_0 + \sum_{i=1}^{6} a_i \sin(b_i + c_i T_0) \quad (22)$$

$$\delta = \sum_{i=1}^{4} d_i \sin(e_i + f_i T_0) \quad (23)$$

Where:

T_0 = Number of Julian centuries since J2000 (01/01/2000)

λ = Lunar ecliptic longitude

δ = Lunar ecliptic latitude

ε_m = Lunar obliquity to the ecliptic plane

The obliquity to the ecliptic plane is then calculated

$$\varepsilon_m = 23.439° - 0.0130042T_0 \quad (24)$$

Next, the horizontal parallax is computed, in order to calculate the Moon's displacement magnitude. The figure below visualises how the horizontal parallax angle is used to calculate the magnitude of lunar displacement with simple trigonometry, this is possible because the system is being considered in the ecliptic plane, and can be flattened to 2 dimensions.

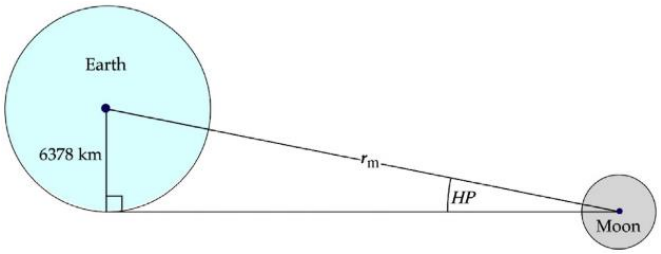

$$r_m = \frac{R}{\sin HP} \quad (25)$$

Figure 30 - Diagram showing the trigonometric relation of the Horizontal Parallax[6]

$$HP = g_0 + \sum_{i=1}^{4} g_i \cos(h_i + k_i T_0) \quad (26)$$

Finally, the geocentric lunar position vector is calculated using the ecliptic longitude, latitude, and obliquity.

$$\boldsymbol{r}_m = r_m \cos\delta \cos\lambda\, \hat{\boldsymbol{\imath}} + r_m(\cos\varepsilon \cos\delta \sin\lambda - \sin\varepsilon \sin\delta)\hat{\boldsymbol{\jmath}} + r_m(\sin\varepsilon \cos\delta \sin\lambda + \cos\varepsilon \sin\delta)\hat{\boldsymbol{k}} \quad (27)$$

A similar process is used for acquiring the position of the Sun, shown below[6].

First, the mean solar longitude, and mean solar anomaly are calculated.

$$L_s = 280.459° + 0.98564736°n \quad (28)$$

$$M_s = 357.529° + 0.98560023°n \quad (29)$$

Where:

n = Number of Julian days since J2000

L_s = Mean solar longitude

M_s = Mean solar anomaly

λ_a = Apparent solar longitude

These values are used to compute the apparent solar longitude, as observed from Earth.

$$\lambda_a = L + 1.915° \sin M + 0.02° \sin 2M \quad (30)$$

The Sun's displacement magnitude can now be computed using the mean anomaly.

$$r_s = (1.00014 - 0.01671\cos M - 0.0014\cos 2M)AU \quad (31)$$

The Sun's obliquity to the geocentric plane is then calculated.

$$\varepsilon_s = 23.439 - 3.56 \times 10^{-7} n \quad (32)$$

Finally, the Solar position vector can be calculated.

$$\hat{\boldsymbol{u}}_s = \cos\lambda\,\hat{\boldsymbol{\imath}} + \sin\lambda\cos\varepsilon\,\hat{\boldsymbol{\jmath}} + \sin\lambda\sin\varepsilon\,\hat{\boldsymbol{k}} \quad (33)$$

a	b	c	d	e	f	g	h	k
	218.32	481267.881				0.9508		
6.29	135	477198.87	5.13	93.9	483202.03	0.05	135	477198.87
-1.27	259.3	-413335.36	0.28	220.2	960400.89	0.0095	259.3	-413335.3
0.66	235.7	890534.22	-0.28	318.3	6003.15	0.0078	253.7	890534.22
0.21	269.9	954397.74	-0.17	217.6	-407332.2	0.0028	269.9	954397.7
-0.19	357.5	35999.05						
-0.11	106.5	966404.03						

Table 4 - List of coefficients for Luni/Solar positioning equations[6]

2.3 Solar Radiation Pressure

Direct solar radiation pressure (SRP) has been shown to have a significant perturbing effect on satellites in MEO, this is modelled using the cannonball approximation in this model, whereby the shape of the satellite is removed as a variable, and the effect of SRP on the satellite is simplified to a single parameter, its area to mass ratio. The equation for the acceleration due to SRP is given below[6].

$$\boldsymbol{a}_{srp} = -v\frac{S}{c}C_r A_{ratio}\hat{\boldsymbol{u}}_{srp} \quad (34)$$

Where:

$\mathbf{a}_{srp}$ = SRP perturbing acceleration vector

v = Shadow function (v = 0 or 1)

S = Solar constant (1367W/m^2)

c = Speed of light (299,792,000 m/s)

C_r = Coefficient of reflectivity (assumed to be 2)

A_{ratio} = Satellite's area/mass ratio (m^2/kg)

$\mathbf{U}_{srp}$ = SRP direction vector, from the Sun to satellite.

In order for SRP to be included accurately in the model, the position of the sun relative to the satellite must be computed to determine whether the satellite is in Earth's shadow and subsequently being acted on by SRP, or not.

This is done by constructing a line that passes through the position of the Sun and the satellite, setting the equation of this line equal to the equation of

a sphere with the equivalent radius of Earth, and solving for the discriminant of the resulting polynomial to determine if the line passes through the Earth and hence if the satellite is in Earth's shadow.

3.0 Implementation

To solve the derived equations of motion for the satellite and acquire results, a numerical integration scheme, implemented in MATLAB, was used. MATLAB's built-in ODE113 ordinary differential equation solver was used to numerically integrate the equations, this was chosen as it showed faster solve times over other solvers, and is listed as possibly being "more efficient than ODE45 at problems with stringent error tolerances, or when the ODE function is expensive to evaluate"[7], two conditions present in this problem.

3.1 Numerical Integration Scheme

Before the derived equations can be integrated, some manipulation must be done for them to be compatible. In this problem the equations and integrator are configured to use a cartesian coordinate system, equation 1, is divided through by the satellite's mass to yield the resulting acceleration on the satellite, and is vectorised and split into a system of 3, 2^{nd} order differential equations describing the acceleration of the satellite along each of the 3 cartesian axes. The equations are then split into a system of 6, 1^{st} order equations describing the acceleration and velocity, using the chain rule.

Accurate computation and handling of the time and timestep are of great importance for the accuracy of the results, hence the concept of Julian dates is utilised, this is a quantity defined as the number of days since January 1^{st}, 4713BC, similar to UNIX time, and is used as the datum in this problem. This allows easy conversion between normal date/time formats and a high accuracy numerical time format for use with the solver software.

The positions of the Sun, Moon, and SRP shadow function are all updated at each timestep in the model, to ensure accurate results.

3.2 Initial Conditions

A wide range of initial orbital conditions were propagated with the model to build a hypothetical "map" of the satellite's orbital lifetime, across the MEO region. To define the deorbited state of a satellite, the condition was set for an orbital altitude of 400km, at this altitude, the satellite is considered to have deorbited due to atmospheric drag and the simulation is ended. All simulations had a starting epoch of 01/01/2021 and were allowed to propagate for a maximum of 200 years. The tolerances for the solver were 1e-11 for both the absolute and relative tolerance.

Orbital Element	Parameter Range	Parameter Step Size
Semimajor axis	25,000km – 30,000km	250km (21 steps)
Eccentricity	0.001 – 0.6	0.03 (21 steps)
Inclination	55° - 65°	2° (6 steps)
Ascending Node	0°, 90°	90° (2 steps)
Argument of Periapsis	0 for all	
True Anomaly	0 for all	
SRP Coefficient	0.015, $1m^2/kg$	
Total number of Orbits	10,584	

Table 5 - List of all Initial conditions and Step sizes for the model

3.3 Optimisation of the model

As there are a very large number of orbits to be propagated, along with a computationally expensive model used, the software model must be optimised as much as possible to decrease computation time. This was achieved by a variety of optimisation methods. Eliminating computation overhead by removing all unnecessary variables and calculations, as well as hardcoding constants and unchanging variables into functions. MATLAB's Parallel Computing Toolbox was also utilised to speed up computation time, due to the nature of numerical integration, it is impossible to parallelise the workload as each timestep requires the known results from the previous step, confining the workload to a serial flow. However, the workload of solving all of the initial conditions was parallelised across multiple threads, decreasing compute time significantly. With this optimisation effort and with the model running on a fairly fast machine (8 cores) the model completed the propagation of 10,584 orbits in approximately 80 hours, reduced from a previously unfeasible completion time.

3.4 Data Handling

The results from the model are in the form of a displacement and state vector describing the satellites orbital condition at each timestep of the integrator, these were saved in a plain text file for analysis. With a large number of orbits simulated, 1 in every 100 timesteps was saved in order to reduce file size. Interpreting the results was done using contour plots of the orbital elements with the colour contour representing the orbital lifetime of the satellite, to easily visualise the relationship between the initial orbital conditions and the satellite's time before de-orbit.

3.5 Validation of the Results

To validate that the model was producing accurate results and was free of any errors, a set of known results for a set of known initial conditions for effects of each perturbation source, taken from the textbook "Orbital Mechanics for Engineering Students"[6] was run through the model to test that it was accurate, with the model running with only 1 source of perturbation at a time, to individually validate each part. Plots of the variation of each orbital element against time were used to check the results against those in the textbook, shown below, here the effects of the perturbing forces on the orbital elements can be seen clearly.

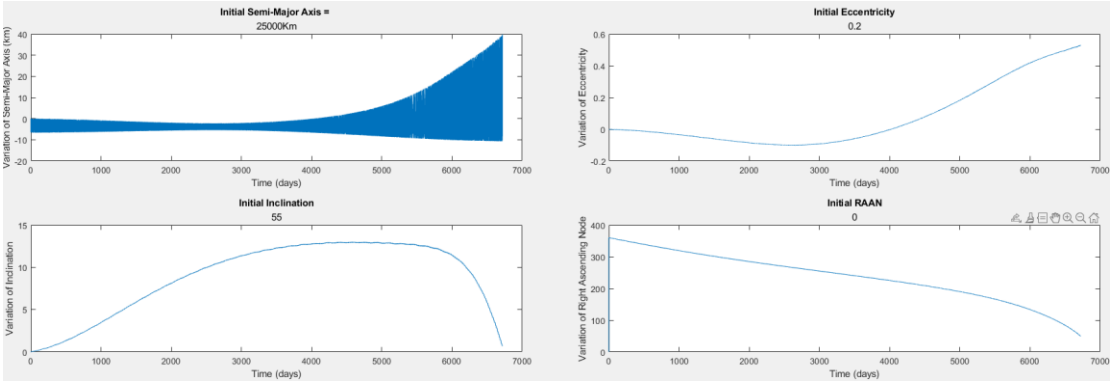

Figure 31 - Plots of Variation of Orbital Elements as a result of Perturbing Forces.

4.0 Discussion

4.1 Results

For a visualisation of the model results, contour plots of the semimajor axis against eccentricity with the colour contour representing the orbital lifetime were generated for each inclination angle and each ascending node angle. This was replicated for each value of SRP area/mass ratio, to allow easy comparison between the values. A set of results for an ascending node angle of 90° and an SRP coefficient of 0.015m^2/kg are shown in figure 7, with an SRP coefficient of 1m^2/kg for figure 8. These plots clearly show a change in the orbital lifetime as a result of different initial conditions, with areas of stability and long lifetime that are consistent with similar shape across changes in inclination, as well as regions with very little stability and a very quick de-orbit time. There is a clear decrease in the overall lifetime as inclination increases, as well as a more random distribution of long lifetime orbital positions.

Comparing figures 7 and 8, it is clear that an increased SRP value does not change the overall structure of the results, but has an enhancing effect, present with even more significance at lower inclinations, resulting in an increased number of fast de-orbits for satellites with high eccentricity with an inclination of 55° and 61° especially. There is a visible trend in the figures showing SRP as the cause of faster de-orbit times for low eccentricity (circular) orbits particularly at higher inclinations, it is clear that the effect of SRP is very complex and is extremely dependent on the initial conditions.

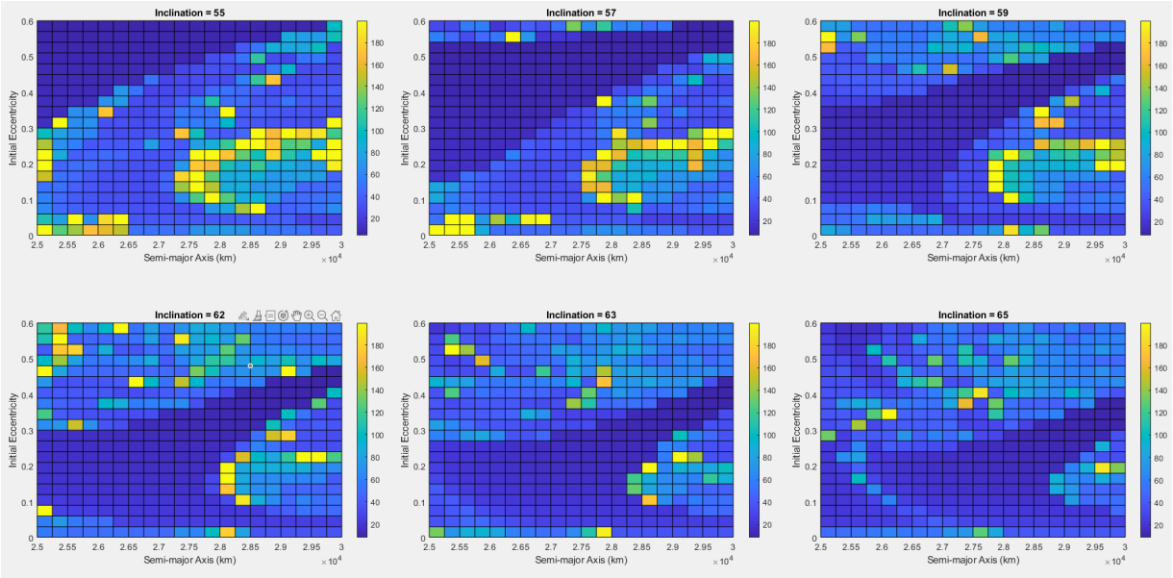

Figure 32 - Contour Plots of Lifetime of Satellites with respect to Initial Semimajor Axis and Eccentricity (A_{ratio} = 0.015m^2/kg, Ascending node = 90°)

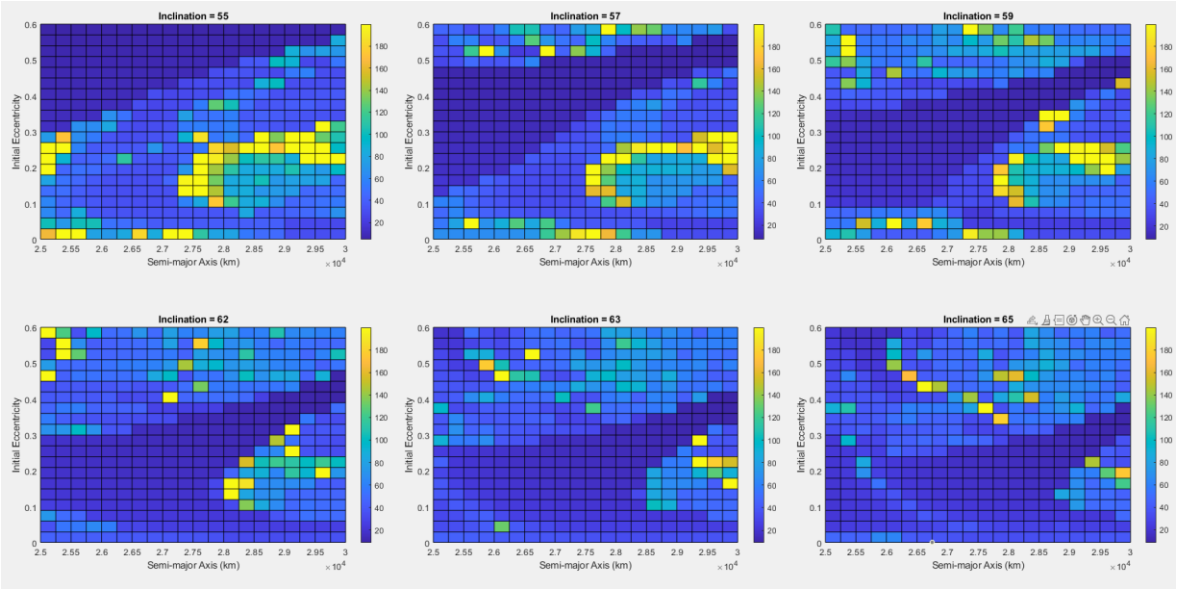

Figure 33 - Contour Plots of lifetime of Satellites with respect to Initial Semimajor Axis and Eccentricity (A_{ratio} = 1m^2/kg, Ascending node = 90°)

4.2 Limitations

This project succeeded in its goal to investigate and analyse the orbital lifetime of GNSS satellites in MEO across different orbital conditions, however, it was limited in terms of access to computational power, and available time, the use of a very powerful machine or supercomputer could enable the generation of much more accurate results across an even wider range of initial conditions.

5.0 Conclusions

This paper aimed to investigate the orbital lifetime of GNSS satellites with high accuracy, and after analysing the available literature to determine the important perturbing forces at play and developing an appropriate orbit propagation model, the results show a clear map of the orbital stability and lifetime of satellites in the GNSS MEO region. This paper found that the relationship between de-orbit time and initial conditions is complex, however displays some general trends, or “hotspots” of stability for certain conditions. These results are useful for the mitigation of space debris, as they allow for the prediction of de-orbit time for static debris already in orbit, and for the prediction of the lifetime of satellites yet to be in service, for their end-of-life procedure to be optimised, and the satellites to be de-orbited easily at the end of their service.

5.1 Future work

This paper covers a very narrow region of the orbital space, for an improvement the initial conditions could be expanded to include the LEO and GEO regions, as well as implementing a standard atmosphere model to accurately include the perturbing force of aerodynamic drag at very low altitudes.

A viable de-orbit strategy for satellites is to deploy a solar drag sail that massively increases the area/mass ratio of the body, decreasing its de-orbit time significantly, a model could be developed around this concept to investigate the required sail size for a given satellite.

6.0 References

[1] J.-C. Liou, D. T. Hall, P. H. Krisko, and J. N. Opiela, "doi_10.1016_j.asr.2003.02.027 _ Elsevier Enhanced Reader.pdf," *Adv. Sp. Res.*, vol. 34, no. 5, pp. 981–986, 2004.

[2] D. K. Skoulidou, A. J. Rosengren, K. Tsiganis, and G. Voyatzis, "Cartographic Study of the Meo Phase Space for Passive Debris Removal," *7th Eur. Conf. Sp. Debris*, no. April, pp. 18–21, 2017.

[3] C. Lücking, C. Colombo, and C. R. McInnes, "A passive satellite deorbiting strategy for MEO using solar radiation pressure and the J 2 effect," *62nd Int. Astronaut. Congr. 2011, IAC 2011*, vol. 3, pp. 2167–2177, 2011.

[4] Mathworks, "Visualizing Geoid Height for Earth Geopotential Model 1996," *Mathworks MATLAB Help Center*. https://uk.mathworks.com/help/aerotbx/ug/visualizing-geoid-height-for-earth-geopotential-model-1996.html.

[5] Hyperphysics, "Diagram of Earth's ecliptic plane," *Hyperphysics Mechanics*. http://hyperphysics.phy-astr.gsu.edu/hbase/eclip.html.

[6] H. D. Curtis, "Introduction to Orbital Perturbations," in *Orbital Mechanics for Engineering Students*, 2014, pp. 651–720.

[7] Mathworks, "Choose an ODE Solver - MATLAB," *Mathworks MATLAB Help Center*. https://uk.mathworks.com/help/matlab/math/choose-an-ode-solver.html.